PONTIFICIA UNIVERSIDAD CATÓLICA DEL PERÚ

ESCUELA DE POSGRADO

Polarimetric measurements of single-photon geometric phases

A thesis in candidacy for the degree of Master of Science in Physics
presented by:

Omar H. Ortiz Cabello

Advisor:
Prof. Francisco De Zela

Jury:
Prof. Eduardo Massoni
Prof. Hernán Castillo

Lima, 2017

Resumen

Reportamos medidas polarimétricas de fases geométricas que son generadas por evoluciones de fotones polarizados a lo largo de trayectorias no geodésicas en la esfera de Poincarè. La esencia de nuestro arreglo polarimétrico está en las siete láminas retardadoras que son atravesadas por un haz de fotones individuales. Con este arreglo, cualquier transformación SU(2) puede ser realizada. Explotando la invarianza Gauge de las fases geométricas bajo transformaciones locales U(1), anulamos la contribución dinámica a la fase total, de este modo haciendo que la última coincida con la fase geométrica. Demostramos la insensibilidad de nuestro arreglo bajo distintas fuentes de ruido. Esto hace del arreglo polarimétrico de fotones individuales una herramienta versátil y prometedora para probar la robustez de la fase geométrica frente al ruido.

Abstract

We report polarimetric measurements of geometric phases that are generated by evolving polarized photons along nongeodesic trajectories on the Poincarè sphere. The core of our polarimetric array consists of seven wave plates that are traversed by a single-photon beam. With this array, any SU(2) transformation can be realized. By exploiting the gauge invariance of geometric phases under U(1) local transformations, we nullify the dynamical contribution to the total phase, thereby making the latter coincide with the geometric phase. We demonstrate our arrangement to be insensitive to various sources of noise entering it. This makes the single-beam, polarimetric array a promising, versatile tool for testing robustness of geometric phases against noise.

Acknowledgements

I would like to express my deepest gratitude to my mother Nelly Cabello Ormachea. I am the proud son of a single mother whose efforts put me in this place and time. I am the result of her teachings, everything I am today and everything I will be is because of her.

I would also like to wish my thanks to Professor Francisco De Zela, who trusted a group of students like me the privilege to work with him, his guidance has been indispensable for this endeavor.

To my friends I am sincerely grateful for all the moments shared. There is not enough space here to mention you all, but from physics I must mention Juan Pablo Velasquez, Juan Carlos Loredo and Carlos Argüelles. I would also like to thank my dear brother Roberto Rodriguez.

To my love and soon to be wife Jimena Vargas, I wish to thank you for all the happiness you bring me, all those enriching conversations and most important I wish to thank you for challenging me to be a better person every day. It is a beautiful path the one we are walking together.

Published Material in this Thesis

Partial and final results contained in this thesis work have been published in the following journal articles and proceedings:

J. C. Loredo, O. Ortíz, R. Weingärtner and F. De Zela: Measurement of Pancharatnam's Phase by Robust Interferometric and Polarimetric Methods *Phys. Rev. A* **80** 012113 (2009).

J. C. Loredo, O. Ortíz, A. Ballón and F. De Zela: Measurement of Geometric Phases by Robust Interferometric Methods *J. Phys.: Conf. Ser.* **274** 012140 (2011).

O. Ortíz, Y. Yugra, A. Rosario, J. C. Sihuincha, J. C. Loredo, M. V. Andrés and F. De Zela: Polarimetric measurements of single-photon geometric phases *Phys. Rev. A* **89** 012124 (2014).

Polarimetric measurements of single-photon geometric phases

O. Ortíz,[1] Y. Yugra,[1] A. Rosario,[1] J. C. Sihuincha,[1] J. C. Loredo,[2] M. V. Andrés,[3] and F. De Zela[1]
[1]*Departamento de Ciencias, Sección Física, Pontificia Universidad Católica del Perú, Apartado 1761, Lima, Peru*
[2]*Centre for Engineered Quantum Systems, Centre for Quantum Computer and Communication Technology, and School of Mathematics and Physics, University of Queensland, 4072 Brisbane, Queensland, Australia*
[3]*Departamento de Física Aplicada y Electromagnetismo, Universidad de Valencia, c/Dr. Moliner 50, Burjassot, Valencia, Spain*
(Received 9 October 2013; published 24 January 2014)

We report polarimetric measurements of geometric phases that are generated by evolving polarized photons along nongeodesic trajectories on the Poincaré sphere. The core of our polarimetric array consists of seven wave plates that are traversed by a single-photon beam. With this array, any SU(2) transformation can be realized. By exploiting the gauge invariance of geometric phases under U(1) local transformations, we nullify the dynamical contribution to the total phase, thereby making the latter coincide with the geometric phase. We demonstrate our arrangement to be insensitive to various sources of noise entering it. This makes the single-beam, polarimetric array a promising, versatile tool for testing robustness of geometric phases against noise.

DOI: 10.1103/PhysRevA.89.012124 PACS number(s): 03.65.Vf, 03.67.Lx, 42.65.Lm

I. INTRODUCTION

Even though experiments testing different properties of geometric phases are continuously reported, theoretical developments can expand at such an accelerated pace that experimental testing can be temporarily left behind. This seems to be the case with the subject of geometric phases. Since Berry's seminal work [1], which brought to light the appearance of geometric phases in adiabatically evolving, cyclic quantum processes, there have been considerable generalizations of the subject. From Hannay angles in the classical domain [2] to geometric phases in mixed quantum states subjected to nonunitary and noncyclic evolutions [3–7], the original concept of geometric phases has been widely expanded. Experimental testing is required not only because of fundamental reasons lying at the basis of all empirical sciences, but because experimental input can help us to find the answer to open questions. Notably, the question about a proper, self-consistent definition of a geometric phase for nonunitary evolutions still remains open [8–13]. Similarly, the kind of robustness that geometric phases might have against decohering mechanisms is also an open question of utmost importance, particularly in the realm of quantum computation [14]. It is thus useful to explore as many experimental techniques as possible. One should not refrain from mirroring experiments already performed with one technique and conduct similar experiments based on another independent technique. This can provide not only new insights, but an enlarged versatility as well. Geometric phases are particularly well suited for such an approach, as they notoriously appear in the evolution of two-level systems. Such systems can be realized under manifold situations, i.e., quantal and classical ones. The drawbacks of one technique could then be replaced by some advantages of the other. For example, the physical realization of the qubit as a spin one-half particle, e.g., a neutron, has its counterpart in the realization of the qubit as a polarized photon. While as a source of the former, one needs a nuclear reactor, as a source of the latter, a diode-laser suffices. On the other hand, the versatility reached in experiments with neutrons can outperform that reached with their optical counterparts. A challenge is thereby put on the latter as to how to improve their versatility. We have addressed such a challenge in the present work. We report on experiments performed with single photons, which to some extent mirror previous experiments that were conducted with neutrons [15–18]. Our experiments put under test theoretical predictions about SU(2) evolutions along nongeodesic paths. Using neutrons, experiments along these lines have been conducted by exploiting the advantages offered by polarimetric techniques. In contrast to interferometric techniques [19], polarimetric ones have an intrinsic robustness because they require a single beam [20]. The challenge posed here, however, is how to manipulate two coherently superposed states that are not spatially separated. In interferometry, the (binary) path degree of freedom can be used together with an "internal" degree of freedom, e.g., the spin, that is carried along by the particle. In polarimetry, instead, there is only one path. One must then figure out how to deal with this restriction and nevertheless reach a versatility that is comparable to that of interferometry. The latter offers, for example, the possibility of spin-path entanglement. In neutron polarimetry, energy-polarization entanglement and even a tripartite energy-polarization-momentum entanglement have been achieved [21]. Although an all-optical version of the latter seems difficult to implement, there are other features that can be exploited with advantage in optical polarimetry. We show here how to exploit the invariance of geometric phases under local gauge transformations [22] in order to nullify the dynamical part of the total (Pancharatnam) phase [23], thereby making this phase coincide with the geometric phase. What is meant by gauge invariance is the invariance under the change $|\psi(s)\rangle \rightarrow |\psi'(s)\rangle = \exp[i\alpha(s)]\,|\psi(s)\rangle$ of an unitarily evolving state $|\psi(s)\rangle$. By exploiting this invariance, one can nullify the dynamical contribution to the total phase, $\Phi_P = \arg\langle\psi(s_1)|\psi(s_2)\rangle$, between an initial and a final state, $|\psi(s_1)\rangle$ and $|\psi(s_2)\rangle$, respectively. What remains after elimination of the dynamical part is the purely geometric contribution Φ_g to the total phase, $\Phi_P = \Phi_g + \Phi_{\rm dyn}$. The SU(2) evolutions we have addressed are those of the type given by $U_n(\theta,\varphi,s) = \exp[-is\mathbf{n}(\theta,\varphi)\cdot\boldsymbol{\sigma}/2]$. Here, $\mathbf{n}$ is a unit vector, $\boldsymbol{\sigma}$ is the triple of Pauli matrices, and s is the

rotation angle (on the Bloch or Poincaré sphere). We could generalize our approach so as to deal with unit vectors that depend on s, but we have focused on cases with a fixed $\mathbf{n}$. We also restricted ourselves to deal with pure single-photon states. These restrictions are justified in view of the extension already achieved by considering the production of geometric phases in systems subjected to transformations $U_n(\theta,\varphi,s)$ of the above type. Previous experimental tests were restricted to particular trajectories that a system follows when subjected to some special transformations [15,17,18]. The cases we address here let us study what happens when we lift these restrictions. In such a case, a series of features shows up that is worthwhile to analyze before undertaking a systematic investigation of, say, the sensitivity of geometric phases to environmental influences. A main motivation of the present work was to analyze and explain the appearance of the aforementioned features. This opens the way for using this array as a basic component for testing the impact of decohering mechanisms.

II. POLARIMETRY

The standard procedure to exhibit the relative phase between two states is to make them interfere and then record the intensity of the interfering pattern by varying the relative phase. An archetypical setup for doing this is a Mach-Zehnder interferometer. Expressed in the language of quantum gates [24], such a device consists of two Hadamard gates—i.e., two beam splitters—and a phase shifter. A Hadamard gate can be represented in terms of Pauli matrices as $U_H = (\sigma_x + \sigma_z)/\sqrt{2}$, while the phase shifter can be represented as $U_\phi = \exp(-i\phi\sigma_z/2)$. Hereby, we establish a one-to-one correspondence between the eigenvectors $|\pm\rangle$ of σ_z and the two paths of the interferometer. The action of the interferometer on an input state $|+\rangle$ is thus given by $|+\rangle \to U_H U_\phi U_H |+\rangle$. The output intensity that is recorded at, say, a $|+\rangle$ detector reads $I = |\langle +|U_H U_\phi U_H|+\rangle|^2 = (1+\cos\phi)/2$. Now, instead of assigning the states $|\pm\rangle$ to the two possible paths of the interferometer, we can make them correspond to the horizontal and vertical polarization states of a single light beam. We thereby change from interferometry to polarimetry. In the latter, the action of U_ϕ and U_H can be realized with the help of quarter-wave (Q) and half-wave (H) plates. Indeed, we have that $U_\phi = Q(\pi/4)H((\phi-\pi)/4)Q(\pi/4)$ and $U_H = -iH(\pi/8)$. The arguments in H and Q refer to the angles made by the plate's major axis and the vertical direction. Up to a global phase, the action of the Mach-Zehnder interferometer can then be mirrored in polarization space by letting a polarized light beam traverse a gadget that consists of a couple of aligned retarders. In the present case, such an array is given by $Q(\pi/2)H((2\pi-\phi)/4)Q(\pi/2)$. This last expression is obtained by using $Q(\alpha)H(\beta) = H(\beta)Q(2\beta-\alpha)$ and $Q(\alpha)H(\beta)H(\gamma) = Q(\alpha+\pi/2)H(\alpha-\beta+\gamma-\pi/2)$. Hence, by setting a horizontal polarizer before a detector and recording the intensity as a function of ϕ, we get a pattern that looks the same as the interferogram produced with the Mach-Zehnder device. Polarimetry has the great advantage of being largely insensitive to those perturbations that in the case of interferometry lead to random phase shifts. On the other hand, the states $|\pm\rangle$ cannot be individually addressed, as they are no longer spatially separated from one another, as occurs in interferometry. We must then find a way to extract the desired information by adequately projecting the manipulated states before detection. In the case of geometric phases, this is indeed possible, as we show next.

Following a similar procedure as the one introduced by Wagh and Rakhecha [20]—thereby extending to single photons some techniques already employed with classical light [25–27]—we consider an initial, horizontally polarized state $|h\rangle$ and submit it to a $\pi/2$ rotation around the x axis. This produces a circularly polarized state $(|h\rangle - i\,|v\rangle)/\sqrt{2}$. By submitting this state to the transformation $\exp(-i\phi\sigma_z/2)$, we get $V|h\rangle \equiv \exp(-i\phi\sigma_z/2)\exp(-i\pi\sigma_x/4)|h\rangle$, which is the state $(|h\rangle - ie^{i\phi}|v\rangle)/\sqrt{2}$, up to a global phase. Hence, we have generated a relative phase shift $\phi - \pi/2$ between $|h\rangle$ and $|v\rangle$. If we now apply $U \in \mathrm{SU}(2)$, we then obtain $UV|h\rangle = (e^{-i\phi/2}U|h\rangle - ie^{i\phi/2}U|v\rangle)/\sqrt{2}$. We are interested in $U_n(\theta,\varphi,s) = \exp[-is\mathbf{n}(\theta,\varphi)\cdot\boldsymbol{\sigma}/2]$ and the geometric phase that this transformation generates. We recall that the geometric phase is given by [22]

$$\Phi_g(\mathcal{C}) = \arg\langle\psi(0)|\psi(s)\rangle - \mathrm{Im}\int_0^s \langle\psi(s')|\dot{\psi}(s')\rangle ds', \qquad (1)$$

for a path $\mathcal{C}$ joining the initial state $|\psi(0)\rangle$ with the final state $|\psi(s)\rangle$. As already said, Φ_g is invariant under local gauge transformations. We exploit this property in order to nullify the dynamical contribution to Φ_g. That is, we choose a gauge transformation $|\psi(s)\rangle \to |\psi'(s)\rangle = \exp[i\alpha(s)]|\psi(s)\rangle$ so that $\langle\psi'(s)|\dot{\psi}'(s)\rangle = 0$. In other words, instead of applying $U_n(\theta,\varphi,s)$, we apply $\exp[i\alpha(s)]\,U_n(\theta,\varphi,s)$ and measure the total phase $\arg\langle\psi(0)|\psi(s)\rangle$. In the present case, this can be achieved by setting $\alpha(s) = s\,\langle+|\,\mathbf{n}\cdot\boldsymbol{\sigma}\,|+\rangle/2$. That is, we seek to implement the transformation $|h\rangle \to U_n V|h\rangle = (e^{-i\gamma/2}U_n|h\rangle - ie^{i\gamma/2}U_n|v\rangle)/\sqrt{2}$, where $\gamma(s) = \phi - \alpha(s)$. We can realize this with the help of wave plates. To begin with, U_n can be implemented with a gadget proposed by Simon and Mukunda [28], which is given by

$$U_n(\theta,\varphi,s) = Q\left(\frac{\pi+\varphi}{2}\right)Q\left(\frac{\theta+\varphi}{2}\right) \times H\left(\frac{-\pi+\theta+\varphi}{2}+\frac{s}{4}\right)Q\left(\frac{\theta+\varphi}{2}\right)Q\left(\frac{\varphi}{2}\right). \qquad (2)$$

The rotation axis is here given by $\mathbf{n} = (\sin\theta\cos\varphi, \sin\theta\sin\varphi, \cos\theta)$ and the Pauli matrices are defined according to the convention that is commonly employed in optics. That is, the diagonal matrix in the basis $\{|h\rangle,|v\rangle\}$ of horizontally and vertically polarized states is σ_x. The other two Pauli matrices follow from cyclically completing the change $\sigma_z \to \sigma_x$. With this choice, our gauge is given by

$$\alpha(s) = \frac{s}{2}\sin\theta\cos\varphi. \qquad (3)$$

On the other hand, $V(\gamma) = e^{-i\gamma\sigma_z/2}e^{-i\pi\sigma_x/4}$ can be implemented as $V(\gamma) = Q(\pi/4)H((\gamma-\pi)/4)H(\pi/4)$. The total transformation is thus

$$U_{\mathrm{tot}} \equiv V^\dagger U_n V = H\left(-\frac{\pi}{4}\right)H\left(\frac{\gamma+\pi}{4}\right)Q\left(-\frac{\pi}{4}\right) \times U_n(\theta,\varphi,s)Q\left(\frac{\pi}{4}\right)H\left(\frac{\gamma-\pi}{4}\right)H\left(\frac{\pi}{4}\right). \qquad (4)$$

Applying as before relations such as $Q(\alpha)H(\beta) = H(\beta)Q(2\beta-\alpha)$, $Q(\alpha)H(\beta)H(\gamma) = Q(\alpha+\pi/2)H(\alpha-\beta+\gamma-\pi/2)$, etc., we reduce the above array to one that consists of seven plates:

$$U_{\rm tot}(\theta,\varphi,\phi,s) = Q\left[\frac{\pi}{4}-\frac{\gamma_\phi(s)}{2}\right]Q\left[-\pi-\frac{\varphi}{2}-\frac{\gamma_\phi(s)}{2}\right]Q\left[\frac{\pi-\theta-\varphi}{2}-\frac{\gamma_\phi(s)}{2}\right]H\left[\frac{-\theta-\varphi}{2}-\frac{s}{4}-\frac{\gamma_\phi(s)}{2}\right]$$
$$\times Q\left[\frac{\pi-\theta-\varphi}{2}-\frac{\gamma_\phi(s)}{2}\right]Q\left[\frac{\pi-\varphi}{2}-\frac{\gamma_\phi(s)}{2}\right]Q\left[-\frac{\pi}{4}-\frac{\gamma_\phi(s)}{2}\right], \tag{5}$$

where $\gamma_\phi(s) = \phi - \alpha(s)$. We use this notation to emphasize that γ depends on both ϕ and s. Note that by going from Eq. (4) to Eq. (5), the gauge-fixing role—originally played by the plates implementing $V(\gamma)$—turns to be shared by all seven plates of the final array. The path followed by the polarization state subjected to $U_{\rm tot}$ can be represented on the Poincaré sphere by a circular arc; see Fig. 1. This arc is fixed by $\mathbf{n}(\theta,\varphi)$, by the initial polarization state, and by s. The latter fixes the angle by which the initial state is rotated. Once we have fixed $\mathbf{n}$ and the initial state, we record the geometric phase as a function of s. This is done by varying the registered intensity as a function of $\gamma_\phi(s)$, which plays a double role. First, it contains the phase shift ϕ that is required to implement the polarimetric version of the Mach-Zehnder interferometer, as discussed above. Second, it contains the gauge shift $\alpha(s)$ that is required to make the total phase coincide with the geometric phase. In order to extract this geometric phase, we project the state $U_n V(\gamma)\,|h\rangle$ onto the state $V(\gamma)\,|h\rangle = e^{-i\gamma/2}(|h\rangle - ie^{i\gamma}\,|v\rangle)/\sqrt{2}$. The recorded intensity is thus given by $I = |\langle h|V^\dagger(\gamma)U_n V(\gamma)|h\rangle|^2$. As we shall see, after having fixed θ, φ, and s, we can let γ (viz., ϕ) vary so as to generate an intensity pattern $I(\phi)$, whose maxima and minima determine the value of the geometric phase at (s,θ,φ). This value can be compared with the theoretical one, which is given by $\Phi_g = \Phi_P - \Phi_{\rm dyn}$, where

$$\Phi_P = \arg\langle\psi(0)|\psi(s)\rangle = \arg\langle h|\,U_n(s)\,|h\rangle$$
$$= -\arctan\left[\sin\theta\cos\varphi\tan\left(\frac{s}{2}\right)\right], \tag{6}$$

$$\Phi_{\rm dyn} = {\rm Im}\int_0^s \langle\psi(s)|\dot{\psi}(s)\rangle ds$$
$$= {\rm Im}\int_0^s \langle h|\,U_n^\dagger(s)(-i\mathbf{n}\cdot\boldsymbol{\sigma})U_n(s)\,|h\rangle\,ds$$
$$= -\frac{s}{2}\,\langle h|\,\mathbf{n}\cdot\boldsymbol{\sigma}\,|h\rangle\,. \tag{7}$$

The theoretical expression for the geometric phase thus reads

$$\Phi_g^{th} = -\arctan\left[\sin\theta\cos\varphi\tan\left(\frac{s}{2}\right)\right] + \frac{s}{2}\sin\theta\cos\varphi. \tag{8}$$

On the other hand, a straightforward calculation of the intensity $I = |\langle h|V^\dagger[\phi-\alpha(s)]U_n(\theta,\varphi,s)V[\phi-\alpha(s)]|h\rangle|^2$ gives

$$I = \cos^2\left(\frac{s}{2}\right) + \sin^2\left(\frac{s}{2}\right)\{\cos\theta\cos[\alpha(s)-\phi]$$
$$+ \sin\theta\sin\varphi\sin[\alpha(s)-\phi]\}^2. \tag{9}$$

We then have

$$I_{\rm min}(s) = \cos^2\left(\frac{s}{2}\right), \tag{10}$$

$$I_{\rm max}(s) = \cos^2\left(\frac{s}{2}\right) + \sin^2\left(\frac{s}{2}\right)[\cos^2\theta + (\sin\theta\sin\varphi)^2], \tag{11}$$

where we have used that the maximum of $f(\alpha) = a\cos\alpha + b\sin\alpha$ is given by $\sqrt{a^2+b^2}$. From the above equations, we get

$$\frac{1-I_{\rm max}}{1-I_{\rm min}} = \sin^2\theta\cos^2\varphi, \tag{12}$$

$$\frac{1-I_{\rm max}}{I_{\rm min}} = \sin^2\theta\cos^2\varphi\tan^2\left(\frac{s}{2}\right). \tag{13}$$

We can thus express Φ_g^{th} in terms of the experimentally accessible quantities $I_{\rm min}$ and $I_{\rm max}$ as

$$\Phi_g(s) = \sqrt{\frac{1-I_{\rm max}(s)}{1-I_{\rm min}(s)}}\,\arccos[\sqrt{I_{\rm min}(s)}]$$
$$-\arctan\left[\sqrt{\frac{1-I_{\rm max}(s)}{I_{\rm min}(s)}}\right] \quad \text{for} \quad -\pi < s < \pi, \tag{14}$$

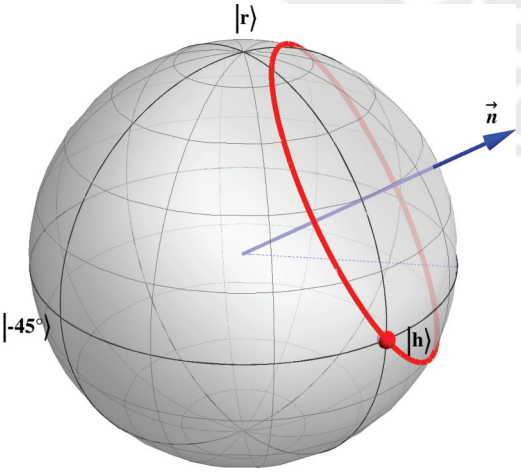

FIG. 1. (Color online) Path followed on the Poincaré sphere by the Stokes vector that corresponds to an initial state $|h\rangle$ being submitted to a transformation $\exp(-is\mathbf{n}\cdot\boldsymbol{\sigma}/2)$. The rotation axis $\mathbf{n}$ has polar angles $\theta = \pi/3, \varphi = \pi/4$. The dynamical contribution to the total phase Φ_P is gauged-away all along the curve, so that $\Phi_P = \Phi_g$ holds at each value of s.

$$\Phi_g(s) = \sqrt{\frac{1 - I_{\max}(s)}{1 - I_{\min}(s)}}\,\arccos[-\sqrt{I_{\min}(s)}] + \arctan\left[\sqrt{\frac{1 - I_{\max}(s)}{I_{\min}(s)}}\right] \pm\pi \quad \text{for} \quad \pi < s < 3\pi. \tag{15}$$

Note that Φ_g is undefined for $s = \pi$; cf. Eq. (8). The $\pm\pi$ that appears in $\Phi_g(s > \pi)$ comes from the Pancharatnam contribution, $\arg\langle h|\, U_n(s)\,|h\rangle$, that is contained in Φ_g^{th}. Indeed, $\langle h|\, U_n(s)\,|h\rangle = \cos(s/2)[1 - i\sin\theta\cos\varphi\tan(s/2)]$, so that $\arg\langle h|\, U_n(s)\,|h\rangle = \arg[\cos(s/2)] - \arctan[\sin\theta\cos\varphi\tan(s/2)]$. For $\pi < s < 3\pi$, we have that $\arg[\cos(s/2)] = \pm\pi$.

III. EXPERIMENTAL PROCEDURE AND ANALYSIS OF RESULTS

A sketch of our experimental arrangement is shown in Fig. 2. Its core is the array of seven plates that realize the transformation $U_{\text{tot}}(\theta,\varphi,\phi,s)$, as given in Eq. (5). Our single-photon source was a beta barium borate (BBO) crystal pumped by a cw diode laser (measured central wavelength 400 nm; spectral linewidth lies between 0.5 and 1 nm at operating temperatures; output power 37.5 mW). Two photon beams were produced in the BBO crystal by type-I spontaneous parametric down-conversion, with each beam having a wavelength of 800 nm. One beam, the idler or heralding one, was directed towards an avalanche photodetector. The other, signal beam, was directed towards the array of seven plates. Coincidence counts (I) of idler and signal beams made up our raw data, with coincidences being defined within a time window of 10.42 ns. Our photon-counting module was a Perkin-Elmer SPCM-AQ4C, with a dark count rate of 500 ± 10 cps. Photons were collected with the help of converging lenses that focused them into multimode fiber-optic cables having fiber-coupling connectors at both ends. The recorded coincidences were obtained according to the following procedure. For given values of θ, φ, and s, the seven plates were oriented as prescribed in Eq. (5), with $\gamma = \phi - s\sin\theta\cos\varphi/2$. The angle ϕ was varied from 0° to 360° in steps of 40°. Coincidence counts were recorded as a function of ϕ and then normalized to obtain the intensity $I(\phi)$. Theoretically, $I(\phi)$ is given by Eq. (9), with s, θ, and φ kept fixed. By repeated measurements, we sampled 30 points for each value of ϕ. The parameter s took values s_i from 40° to 320° in steps of 40°. After averaging the recorded coincidence counts for each ϕ, we obtained a series of points $I(\phi_i)$. A best fit $I(\phi)$ to these points was found, where $I(\phi)$ is a sinusoidal function whose parameters were fixed by the least-squares method. Figure 3 shows the so-obtained curves for $\theta = \pi/2$, $\varphi = \pi/3$ and different values of s. From these curves, we determined $I_{\max}$ and $I_{\min}$. By entering $I_{\max}$ and $I_{\min}$ in Eqs. (14) and (15), the experimental values of $\Phi_g(s,\theta,\varphi)$ can be obtained and compared with the ones predicted by Eq. (8). Figure 4 shows our experimental results together with the corresponding theoretical predictions. As can be seen, two of the three cases seem to reflect a systematic departure of our experimental findings from the theoretical predictions. We will come back to this point below. As for the single-photon production, it was checked by the standard procedure [29,30] of measuring the degree of second-order coherence, $g^{(2)}$, between the output fields of a beam splitter, i.e., the reflected (R) and transmitted (T) beams. Detections at gates T and R were conditioned upon detection at a third gate G. In such a case, $g^{(2)} = P_{GTR}/(P_{GT}P_{GR})$, where the P_a denote probabilities for simultaneous detection at gates specified by label a. In terms of photo counts N_a, the degree of coherence can be expressed as [31] $g^{(2)} = N_{GTR}N_G/(N_{GT}N_{GR})$. It has a value that is less than 1 for nonclassical light. We obtained $g^{(2)} = 0.187 \pm 0.011$ in our experiments.

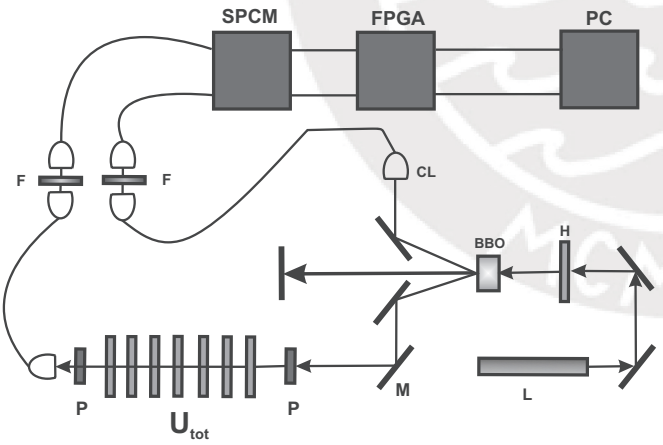

FIG. 2. Polarimetric array. The set of seven wave plates shown at the bottom can be oriented so as to realize the desired SU(2) transformation (U_{tot}) in polarization space. Polarized photons enter this array after having been produced in a nonlinear, beta barium borate (BBO) crystal that is fed by a diode laser (L) that emits 400 nm light whose polarization is fine tuned with a $\lambda/2$ plate (H) placed before the crystal. Polarizers (P) set before and after the retarders project the photon's polarization as required (see text). Signal photons are recorded in coincidence with their heralding twins in a single-photon counting module (SPCM). Other components are M: mirrors; CL: converging lenses; F: filters, FPGA: field programmable gate array; and PC: personal computer.

Several sources of experimental error could be identified. The main source of error came from the accuracy with which our plates could be oriented, i.e., approximately ±1°. Another possible source of error came from our photons having a wavelength of 800 nm instead of the 808 nm that would be required for optimal performance of our wave plates. These are zero-order plates whose effective retardances at the produced wavelength made them slightly differ from being $\lambda/2$ and $\lambda/4$ plates. However, the corresponding departures (0.505λ instead of $\lambda/2$ and 0.253λ instead of $\lambda/4$) were small enough to be neglected as a sensible source of error. Accidental coincidence counts were also estimated to be too small (contribution to $g^{(2)}$ less than 0.19) for them to have a noticeable influence on the departures of our experimental findings from the theoretically predicted values when $s > \pi$ (see Fig. 4, middle and right panels). As illustrated in Fig. 4, left panel, the agreement between the theoretical predictions and measured values was very good. However, we also observed slight departures that occasionally increased. The dashed curves in Fig. 4, middle and right panels, correspond to the targeted geometric phase

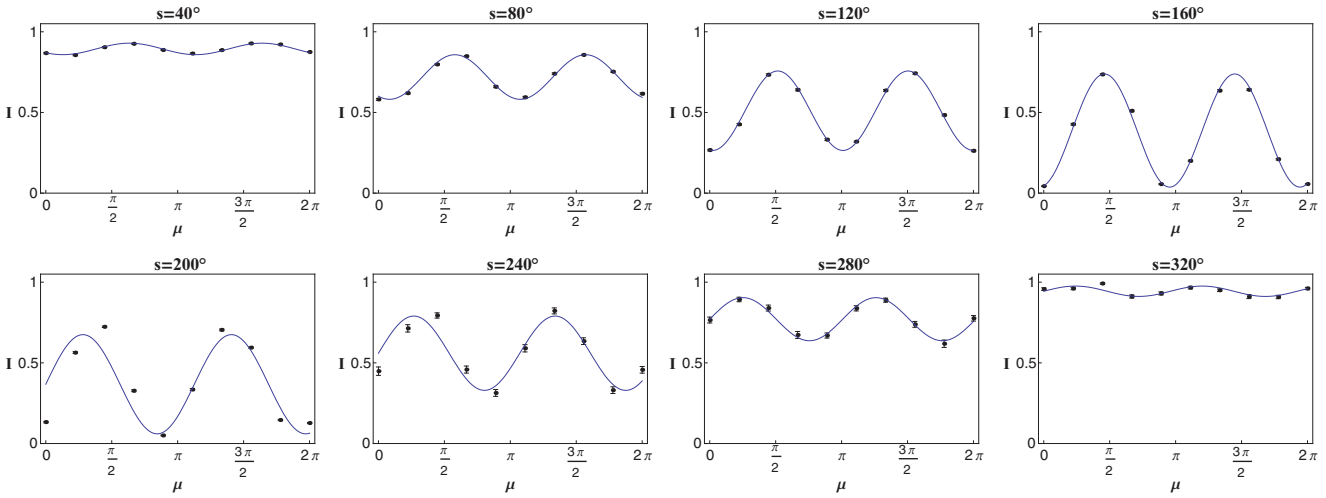

FIG. 3. (Color online) The geometric phase is experimentally fixed by the maxima and minima of the measured curves $I_{\rm exp}(\phi)$. The plotted curves correspond to $\theta = \pi/3$, $\varphi = \pi/3$.

$\Phi_g(s,\theta,\varphi)$. Large departures seemed to reflect a drift of the measured values with respect to the assumed theoretical curve, rather than random fluctuations around this curve. In what follows, we substantiate our claim that the $\pm 1^\circ$ accuracy in the orientation of our plates does explain occasional, systematic departures of experimental measurements from theoretical predictions. Depending on the measured quantity, rotation errors of this magnitude can give rise to inaccuracies of various sorts, such as those recently reported in [32]. It is important to identify error sources and their effects, especially when one's ultimate goal is to have a good understanding of how the geometric phase behaves in a noisy environment.

Let us denote by δ_i the departure of the ith plate's orientation from its nominal value. For a quarter-wave plate, we must then set $Q(x+\delta)$ instead of $Q(x)$ in Eq. (5). To first order in δ, we get $dQ(x) = Q(x+\delta) - Q(x) = \sqrt{2}i\delta R_x$, with

$$R_x = \begin{pmatrix} \sin(2x) & -\cos(2x) \\ -\cos(2x) & -\sin(2x) \end{pmatrix}. \tag{16}$$

Similarly, for a half-wave plate, we obtain $dH(x) = H(x+\delta) - H(x) = 2i\delta R_x$. If we now replace the operators $Q(x)$ and $H(x)$ in Eq. (5) by $Q(x) + dQ(x)$ and $H(x) + dH(x)$, respectively, and then expand the result to first order in the δ_i, we obtain

$$U^\delta_{\rm tot} = U_{\rm tot} + \sum_{i=1}^{7} U^\delta_i, \tag{17}$$

where U^δ_i reads like $U_{\rm tot}$ [see Eq. (5)], except that its ith factor is replaced by $dH(x)$ when $i = 4$ and by $dQ(x)$ otherwise. $U^\delta_{\rm tot}$ is then a function of all $\delta_{i=1,\ldots,7}$. From the amplitude $\langle h|\, U^\delta_{\rm tot}\, |h\rangle$, we can calculate the total intensity $I_\delta = \left|\langle h|\, U^\delta_{\rm tot}\, |h\rangle\right|^2$, once again to first order in the δ_i. With this expression, by choosing different values for the δ_i, we can study how much $I_\delta(\phi)$ differs from the $I(\phi)$ given in Eq. (9). We have found that the departures from I can be very sensitive to a change from, say, $\delta_i \approx +1^\circ$ to $\delta_i \approx -1^\circ$, keeping fixed all the other $\delta_{j\neq i}$. The values of $I_{\rm max}$ and $I_{\rm min}$ can be calculated using $I(\phi)$ and $I_\delta(\phi)$ in order to assess the sensitivity of the array to changes $\delta_i \approx \pm 1^\circ$ in the setting of the plates. The values of $I_{\rm max}$ and

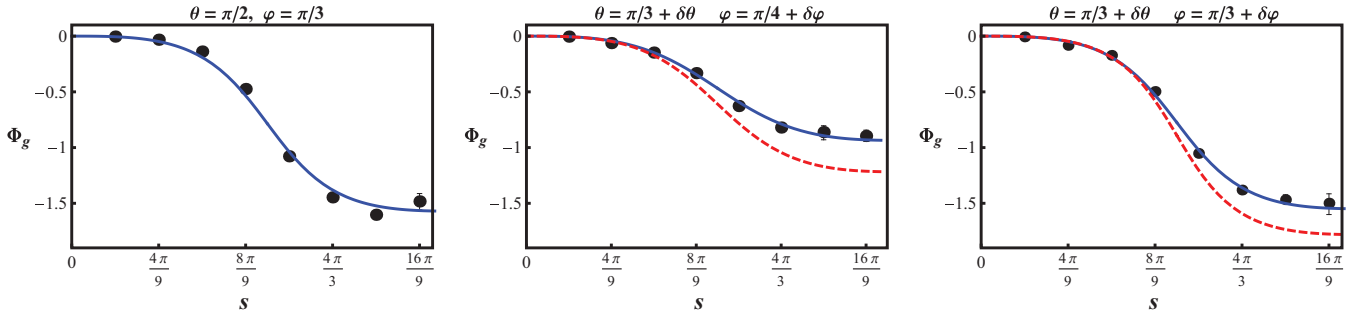

FIG. 4. (Color online) Geometric phase $\Phi_g(s,\theta,\varphi)$ as a function of parameter s for three choices of (θ,φ). Curve $\Phi_g(s,\pi/2,\pi/3)$ closely matches experimental results. However, $\Phi_g(s,\pi/3,\pi/4)$ and $\Phi_g(s,\pi/3,\pi/3)$ seem to systematically deviate from the measured values. By properly identifying the actual values of (θ,φ), the theoretical curves do match experimental results. Dashed curves correspond to $\Phi_g(s,\pi/3,\pi/4)$ (middle panel) and to $\Phi_g(s,\pi/3,\pi/3)$ (right panel). Full curves correspond to $\Phi_g(s,\pi/3+\delta\theta,\pi/4+\delta\varphi)$ with $\delta\theta = 3^\circ\pi/180^\circ$, $\delta\varphi = -7^\circ\pi/180^\circ$ (middle panel) and to $\Phi_g(s,\pi/3+\delta\theta,\pi/3+\delta\varphi)$ with $\delta\theta = 5^\circ\pi/180^\circ$, $\delta\varphi = -4^\circ\pi/180^\circ$ (right panel). Most error bars are smaller than symbols.

$I_{\min}$ that correspond to $I_\delta(\phi)$ show that inaccuracies $\delta_i \approx \pm 1^\circ$ can explain the observed differences between recorded phases and theoretically predicted ones; cf. Eqs. (14) and (15).

The last claim can be confirmed by the following, independent approach. Inaccuracies $\delta_i \approx \pm 1^\circ$ should translate into a departure of θ and φ from their nominal values. Let us then assume that our array does not realize the transformation $U_n(\theta,\varphi,s) = \exp[-is\mathbf{n}(\theta,\varphi)\cdot\boldsymbol{\sigma}/2]$, but instead $\exp[-is\mathbf{n}(\theta+\delta\theta,\varphi+\delta\varphi)\cdot\boldsymbol{\sigma}/2]$, with $\delta\theta \approx \pm 7^\circ \approx \delta\varphi$. The actual values of $\delta\theta$ and $\delta\varphi$ can be obtained by the following procedure. From Eq. (12), we see that $I_{\max}(s_i)$ and $I_{\min}(s_i)$ corresponding to targeted values θ and φ should satisfy

$$y(s_i) \equiv \frac{1 - I_{\max}(s_i)}{1 - I_{\min}(s_i)} = \sin^2\theta\cos^2\varphi \equiv f(\theta,\varphi). \tag{18}$$

The above equation can be used to determine the actual values of θ and φ, i.e., $\theta+\delta\theta$ and $\varphi+\delta\varphi$, by the least-squares method. To this end, we evaluate the right-hand side of Eq. (18) in the sought-after values, expand it to first order, i.e., we set $f(\theta+\delta\theta,\varphi+\delta\varphi) = f(\theta,\varphi) + (\sin 2\theta\cos^2\varphi)\delta\theta - (\sin^2\theta\sin 2\varphi)\delta\varphi$, and then determine $\delta\theta$, $\delta\varphi$ as

$$\begin{pmatrix}\delta\theta\\ \delta\varphi\end{pmatrix} = (A^T W A)^{-1} A^T W b. \tag{19}$$

Here, $(\cdot)^{-1}$ means the Moore-Penrose pseudoinverse, b is the column vector $[y(s_i) - f(\theta,\varphi)]^T$, with $i = 1,\ldots,n$ (n is the number of recorded points), A is the $n\times 2$ matrix whose rows are all equal to $(\sin 2\theta\cos^2\varphi, -\sin^2\theta\sin 2\varphi)$, and W is the inverse of the covariance matrix, i.e., $W = \mathrm{diag}(\sigma_1^{-2},\ldots,\sigma_n^{-2})$. The latter corresponds to statistically uncorrelated measurements having different variances σ_i at different values s_i. We have assessed these variances in two different ways: first by fitting a Gaussian to the distributions of measured points (cf. Fig. 3), which gives us σ_i for each value $I(\phi_j)$ and hence for $I_{\min}$, $I_{\max}$, and Φ_g by error propagation. Second, from our raw data, which consists of 30 values for each ϕ_i – with s, θ, φ being kept fixed, we randomly chose 10 values for each ϕ_i and calculated Φ_g as we did when using the 30 values. By iterating this procedure several times ($\approx$40), we got a series of values for each $\Phi_g(s,\theta,\varphi)$. From each series, we obtained a mean value and its corresponding maximal and minimal departures. These departures constitute our error bars. Such an estimation is justified by the statistical independence of our measurements. Thus, randomly sampling 10 out of 30 measured values amounts to having recorded 10 values in each run of the experiment, while repeating it several times ($\approx$40). From the two methods, we observe that our measured values σ_i span a range that goes from a minimum of 1.3×10^{-4} to a maximum of 0.12. The plotted error bars (cf. Fig. 4) are mostly smaller than the symbols and can barely be seen only in cases for which $\sigma_i \approx 0.1$. Now, the above-mentioned application of the least-squares method holds whenever inaccuracies δs_i of the s_i can be neglected. In our case, the nominal value of s enters in the orientations of our wave plates and the inaccuracies of these orientations are precisely the assumed main source of errors. Nevertheless, the above application of the least-squares method is justified. Indeed, we can assess the values of the δs_i by using Eq. (10). That is, we set $\delta s_i \approx |s_i - 2\arccos(\sqrt{I_{\min}(s_i)})|$ as an estimator of the inaccuracies of the s_i. These inaccuracies turn out to be negligible in comparison to our σ_i—besides, if they were not, they would modify the above results only to higher order than the first in $(\delta\theta,\delta\varphi)$ because our $y(s_i)$ do not depend on s, as Eq. (18) shows. The least-squares method can thus be iteratively applied to find successive values of $\delta\theta$ and $\delta\varphi$, until $\Phi_g^{th}(s,\theta+\delta\theta,\varphi+\delta\varphi)$ of Eq. (8) eventually matches experimental results. In the present case, however, it proved more practical to seek the right choice of θ and φ by hand, i.e., by trial and error when plotting $\Phi_g^{th}(s,\theta+\delta\theta,\varphi+\delta\varphi)$ together with its measured values. Indeed, by doing so in the cases of Fig. 4, middle and right panels, we quickly found values $\delta\theta \approx \pm 7^\circ \approx \delta\varphi$ for which the theoretical curves very closely approximate our experimental results. Figure 4 shows the curves obtained with $\delta\theta = 3^\circ$, $\delta\varphi = -7^\circ$ (middle panel) and $\delta\theta = 5^\circ$, $\delta\varphi = -4^\circ$ (right panel). Such a result is consistent with the assumed errors $\delta_i \approx \pm 1^\circ$, which may accumulate so as to produce inaccuracies $\delta\theta \approx \pm 7^\circ \approx \delta\varphi$. Thus, departures of θ and φ from their targeted values do explain our experimental findings. We have thereby assessed the amount by which the theoretically predicted value $\Phi_g^{th}(s,\theta,\varphi)$ might differ from the experimentally realized one. Such a difference should be taken into account when assessing, with the help of a polarimetric array, the robustness of Φ_g against decohering mechanisms.

Finally, let us point out the following feature of our array. As can be seen from Eqs. (14) and (15), the geometric phase we produce depends on θ and φ only through $|\sin\theta\cos\varphi|$. This means that we can fix the actually realized values of θ and φ only up to changes $(\theta,\varphi) \to (\theta',\varphi')$ that leave $|\sin\theta\cos\varphi|$ invariant. Instead of seing this as a weakness of our approach, such a feature can be helpful when seeking to exploit the robustness of Φ_g against decoherence. Indeed, if one is able to confine decohering effects to those regions in the plane (θ,φ) for which the variations in $|\sin\theta\cos\varphi|$ are sufficiently small, then Φ_g will vary also within acceptable limits. Of course, these limits will depend on the application one has in mind and on the decohering mechanisms, which should be studied in detail. Such an endeavor goes beyond the scope of the present paper and is deferred to future work.

IV. CONCLUSIONS

Our polarimetric setup proved to be a versatile tool for testing geometric phases. The main part of it, an array made of one $\lambda/2$ and six $\lambda/4$ plates, allows us to realize geometric phases that are associated to nongeodesic paths on the Poincaré sphere. Although we have limited ourselves to study circular trajectories, our approach can be extended to deal with arbitrary paths. Our experimental results fit very closely with the theoretical predictions once we have accurately identified the trajectory on the Poincaré sphere that has been actually realized by our setting. The end product of such a setting is a geometric phase Φ_g that is nontrivially related to various parameters entering our setup. Indeed, coincidence counts must be optimized by adjusting the laser polarization, the acquisition window for photon counts must also be properly fixed, and the wave plates must be repeatedly set to their nominal orientations when recording the data from which Φ_g can be extracted. Not only because of the photon-counting statistics but mainly because of our $\pm 1^\circ$ accuracy in the

setting of the plates, one could expect experimental results falling within some region around the theoretical curves, as reported, e.g., in [32]. If that were the case, our polarimetric array would have proven to be inappropriate for studying the robustness of geometric phases against noise. However, our array does produce geometric phases that are in accordance with theoretical expressions. Occasionally, these expressions must be evaluated *a posteriori*, thereby identifying the actually realized values of the parameters fixing Φ_g. Once the value of Φ_g has been fixed, our array can be used for assessing the robustness of this Φ_g against noise. To this end, the array must be complemented so as to simulate different kinds of noise. For instance, one can replace the single-crystal photon's source and use instead polarization-entangled photons produced by parametric down-conversion in a two-crystal geometry [33,34]. This produces variable entangled polarization states. After tracing over the polarization of one of these photons, its twin photon is brought into a mixed polarization state $\rho = (\mathbb{1} + r\mathbf{n}\cdot\boldsymbol{\sigma})/2$, with $r \in [0,1]$ being the degree of polarization. Such a state can be submitted to a polarimetric array similar to the one discussed in this paper. Now, ρ can be written in the form $\rho = \lambda_+|\mathbf{n}_+\rangle\langle\mathbf{n}_+| + \lambda_-|\mathbf{n}_-\rangle\langle\mathbf{n}_-|$, with $\lambda_\pm = (1 \pm r)/2$ and $\mathbf{n}\cdot\boldsymbol{\sigma}|\mathbf{n}_\pm\rangle = \pm|\mathbf{n}_\pm\rangle$. Applying to $|\mathbf{n}_\pm\rangle$ the techniques of the present work, one can get the corresponding (pure-state) geometric phases $\pm\Phi_g$. This is all one needs [35] to obtain the geometric phase of the mixed state ρ, thereby assessing the effect of noise. Experiments along these lines have already been performed in neutron polarimetry [17,18]. The kind of noise studied in [17] translated into a Stokes vector $\mathbf{r} = r\mathbf{n}$ of the restricted form $\mathbf{r} = (0,-r,0)$, and the explored paths on the Bloch sphere originated from unitary transformations that depended on two of the three Euler angles [17]. By appropriate choice of these two angles, one can generate purely geometric, purely dynamical, or combinations of both phases. However, once this choice is made, one cannot freely address different paths on the Bloch sphere. Nevertheless, these results represented a considerable extension of previous ones [15], which dealt with Pancharatnam's phase only. Further progress in assessing the robustness of geometric phases was achieved by addressing adiabatic evolutions [18]. Here, the dynamical contribution to the total phase was eliminated by spin-echo techniques, which impose some restrictions on the class of paths being explored. Our all-optical setting offers some advantages compared to neutron polarimetry. It allows choosing arbitrary paths on the Poincaré sphere, as well as different kinds of noise to be explored in conjunction with the chosen path. The aforementioned remote state preparation of mixed states is not the only choice. One can also employ interferometric techniques to produce an enlarged family of mixed states [32,36]. By applying interferometry for input-state preparation and polarimetry for state manipulation, one has the possibility of studying the resilience of purely geometric phases to various types of noise.

ACKNOWLEDGMENTS

This work was partially financed by DGI-PUCP (Grant No. 2013-0130). J.C.S. thanks E. J. Galvez for support and advice during his stay at Colgate University.

[1] M. V. Berry, Proc. R. Soc. London A **392**, 45 (1984).
[2] J. H. Hannay, J. Phys. A **18**, 221 (1985).
[3] D. M. Tong, E. Sjöqvist, L. C. Kwek, and C. H. Oh, Phys. Rev. Lett. **93**, 080405 (2004).
[4] J. G. Peixoto de Faria, A. F. R. de Toledo Piza, and M. C. Neves, Europhys. Lett. **62**, 782 (2002).
[5] F. M. Cucchietti, J.-F. Zhang, F. C. Lombardo, P. I. Villar, and R. Laflamme, Phys. Rev. Lett. **105**, 240406 (2010).
[6] A. Uhlmann, Rep. Math. Phys. **24**, 229 (1986).
[7] E. Sjöqvist, A. K. Pati, A. Ekert, J. S. Anandan, M. Ericsson, D. K. L. Oi, and V. Vedral, Phys. Rev. Lett. **85**, 2845 (2000).
[8] K.-P. Marzlin, S. Ghose, and B. C. Sanders, Phys. Rev. Lett. **93**, 260402 (2004).
[9] A. Bassi and E. Ippoliti, Phys. Rev. A **73**, 062104 (2006).
[10] A. T. Rezakhani and P. Zanardi, Phys. Rev. A **73**, 052117 (2006).
[11] S. Yin and D. M. Tong, Phys. Rev. A **79**, 044303 (2009).
[12] N. Burić and M. Radonjić, Phys. Rev. A **80**, 014101 (2009).
[13] F. C. Lombardo and P. I. Villar, Phys. Rev. A **81**, 022115 (2010).
[14] E. Sjöqvist, Physics **1**, 35 (2008).
[15] J. Klepp, S. Sponar, Y. Hasegawa, E. Jericha, and G. Badurek, Phys. Lett. A **342**, 48 (2005).
[16] R. A. Bertlmann, K. Durstberger, Y. Hasegawa, and B. C. Hiesmayr, Phys. Rev. A **69**, 032112 (2004).
[17] J. Klepp, S. Sponar, S. Filipp, M. Lettner, G. Badurek, and Y. Hasegawa, Phys. Rev. Lett. **101**, 150404 (2008).
[18] S. Filipp, J. Klepp, Y. Hasegawa, C. Plonka-Spehr, U. Schmidt, P. Geltenbort, and H. Rauch, Phys. Rev. Lett. **102**, 030404 (2009).
[19] S. Werner, Found. Phys. **42**, 122 (2012).
[20] A. G. Wagh and V. C. Rakhecha, Phys. Lett. A **197**, 112 (1995).
[21] S. Sponar *et al.*, New J. Phys. **14**, 053032 (2012).
[22] N. Mukunda and R. Simon, Ann. Phys. (NY) **228**, 205 (1993).
[23] S. Pancharatnam, Proc. Indian Acad. Sci. A **44**, 247 (1956); Reprinted in *Collected Works of S. Pancharatnam* (Oxford University Press, Oxford, 1975).
[24] J. Audretsch, *Entangled Systems: New Directions in Quantum Physics* (Wiley-VCH, Chichester, 2007).
[25] J. C. Loredo, O. Ortíz, R. Weingärtner, and F. De Zela, Phys. Rev. A **80**, 012113 (2009).
[26] J. C. Loredo, O. Ortíz, A. Ballón, and F. De Zela, J. Phys.: Conf. Ser. **274**, 012140 (2011).
[27] J. C. Loredo, Master's Thesis, Pontificia Universidad Católica del Perú, Lima-Peru, 2011.
[28] R. Simon and N. Mukunda, Phys. Lett. A **138**, 474 (1989).
[29] P. G. Kwiat and R. Y. Chiao, Phys. Rev. Lett. **66**, 588 (1991).
[30] J. J. Thorn, M. S. Neel, V. W. Donato, G. S. Bergreen, R. E. Davies, and M. Beck, Am. J. Phys. **72**, 1210 (2004).
[31] P. Grangier, G. Roger, and A. Aspect, Europhys. Lett. **1**, 173 (1986).

[32] K. A. G. Fisher, R. Prevedel, R. Kaltenbaek, and K. J. Resch, New J. Phys. **14**, 033016 (2012).
[33] P. G. Kwiat, E. Waks, A. G. White, I. Appelbaum, and P. H. Eberhard, Phys. Rev. A **60**, R773 (1999).
[34] S. P. Walborn, C. H. Monken, S. Pádua, and P. H. Souto Ribeiro, Phys. Rep. **495**, 87 (2010).
[35] P. Larsson and E. Sjöqvist, Phys. Lett. A **315**, 12 (2003).
[36] F. De Zela, J. Opt. Soc. Am. A **30**, 1544 (2013).

Measurement of geometric phases by robust interferometric methods

2011 J. Phys.: Conf. Ser. 274 012140

(http://iopscience.iop.org/1742-6596/274/1/012140)

Journal of Physics: Conference Series **274** (2011) 012140 doi:10.1088/1742-6596/274/1/012140

Measurement of geometric phases by robust interferometric methods

J. C. Loredo, O. Ortíz, A. Ballón and F. De Zela

Abstract. We present a novel interferometric arrangement that makes it possible to measure with great versatility geometric phases produced in polarization states of classical light. Our arrangement is robust against thermal and mechanical disturbances and can be set up in a Mach-Zehnder, a Michelson or a Sagnac configuration. We present results concerning the geometric phase as an extension of previous measurements of the Pancharatnam, or total phase. The geometric phase is obtained by compensating the dynamical contribution to the total phase, so as to extract out of it a purely geometric phase. This can be achieved over trajectories on the Poincaré sphere that are not necessarily restricted to be great circles (geodesics). We thus demonstrate the feasibility of our method for dynamical extraction of the geometric contribution to the total phase, a prerequisite for building geometric quantum gates. Although our results correspond to polarization states of classical light, the same methodology could be applied in the case of polarization states of single photons.

Pontificia Universidad Católica del Perú, Av. Universitaria 1801, San Miguel, Lima, Peru

E-mail: fdezela@pucp.edu.pe

1. Introduction

In a previous paper [1], we have demonstrated the versatility of an interferometric array that allows accurate measurements of the Pancharatnam phase [2] for two arbitrary polarization states. The array was shown to be robust to thermal and mechanical disturbances and could be set up in different configurations, like those corresponding to a Mach-Zehnder, a Sagnac, or a Michelson interferometer. Its robustness was shown to be similar to that of a polarimetric array [3]. Alternative, robust interferometric setups have been recently demonstrated [4]. Although such interferometers were used for other purposes, they could represent a promising alternative to our setup, in case one aims at scaling the latter down, so as to construct a compact device.

Besides being interesting on its own as a feature which exposes a common root underlying different phenomena in quantum and classical physics, the geometric phase could also be a useful tool for quantum computation. This is due to the fact that it is largely immune to those disturbances that usually cause decoherence. As is well known, decoherence is one of the central problems precluding the construction of a quantum computer. Indeed, computational tasks on a qubit should be performed in a time that is short compared to the decoherence time, and this is usually difficult to achieve. A promising route towards the construction of fault-tolerant quantum computers requires having at one's disposal some devices with the help of which one can move a qubit around a parameter space. In this way one could implement quantum gates based on exploiting the capability of manipulating the phase acquired by the qubit as it completes a closed path on the chosen parameter space. This is called geometric (or holonomic) quantum computation. Its theoretical foundations were laid by Zanardi and

Rasetti [5] some years ago. Experimental demonstrations of geometric quantum gates have been reported [6] using nuclear magnetic resonance. Different experimental scenarios have been explored over the last years, like semiconductor quantum dots [7], ion traps [8], and others. The photonic version of geometric gates is a promising candidate because the corresponding setups are relatively cheap and easy to mount and manipulate. They allow testing different configurations that can afterwards be implemented by using other means. We have thus focused on implementing an all-optical array that allows generating and measuring geometric phases connected to, in principle, arbitrary circuits on the Poincaré sphere. This is a distinctive feature of our approach, as compared to previous ones. Indeed, geometric phases have been exhibited almost exclusively using paths consisting on a series of geodesic segments, i.e., great circles on the Poincaré or Bloch spheres. In other cases, special circuits have been proposed, which were chosen so that the dynamical contribution to the total (Pancharatnam) phase vanished, leaving only the geometrical contribution [9]. This approach imposes, of course, undesirable restrictions to the realization of geometrical phases and also puts technical challenges for its implementation. In our case, we are able to nullify the dynamical contribution to the total phase for any chosen path on the Poincaré sphere. Thus, a great versatility is achieved, offering the possibility of choosing the most appropriate path in parameter space for implementing a geometric quantum gate. In particular, this path could be chosen short enough to meet the requirements set by the need of counteracting decoherence effects. Though geometric phases should be largely immune to decoherence, this is a point in need of further investigation [10], something for which our approach also naturally lends itself.

2. The interferometric method for measuring the geometric phase

In what follows, we use Dirac's notation of bras and kets to stress that our results are equally valid for the classical and for the quantum case. A ket $|\psi\rangle$ will thus denote a polarization state, whose general form can be parametrized as

$$|\psi\rangle = \begin{pmatrix} \cos\theta \\ e^{i\varphi}\sin\theta \end{pmatrix}. \tag{1}$$

Pancharatnam's phase Φ_P between two non-orthogonal states, $|i\rangle$ and $|f\rangle$, is defined as $\Phi_P = \arg\langle i|f\rangle$. It can be exhibited through interferometry by applying a phase-shift ϕ to one of the states, so that the resulting intensity pattern is given by

$$I = \left|e^{i\phi}|i\rangle + |f\rangle\right|^2 = 2 + 2\,|\langle i|f\rangle|\cos\left(\phi - \arg\langle i|f\rangle\right). \tag{2}$$

By noting that the maxima of I occur for $\phi = \arg\langle i|f\rangle = \Phi_P$, Pancharatnam gave an operational definition for the phase between two arbitrary – though non-orthogonal – polarization states. We are interested in the case where $|f\rangle = U|i\rangle$, with U being a unitary transformation. Because the states we consider are formally spinors (whose global phase is physically irrelevant), $U \in SU(2)$. Among the different parametrizations of U, the following one is particularly well suited for extracting Pancharatnam's phase:

$$U(\beta,\gamma,\delta) = \exp\left(i(\frac{\delta+\gamma}{2})\sigma_z\right)\exp\left(-i\beta\sigma_y\right)\exp\left(i(\frac{\delta-\gamma}{2})\sigma_z\right), \tag{3}$$

with $\sigma_{i=x,y,z}$ being the Pauli matrices. Indeed, taking $|i\rangle = |+\rangle_z$, i.e., the eigenstate of σ_z that belongs to the eigenvalue $+1$, and setting $|f\rangle = U|+\rangle_z$ we have

$$\langle i|f\rangle = {}_z\langle +|\,U(\beta,\gamma,\delta)\,|+\rangle_z = e^{i\delta}\cos\beta. \tag{4}$$

From $\Phi_P = \arg\langle i|f\rangle$ we obtain $\Phi_P = \delta + \arg(\cos\beta)$. Because $\cos\beta$ can take on positive and negative real values, $\arg(\cos\beta)$ equals 0 or π, and Φ_P is thus obtained modulo π. In principle,

then, we could obtain Φ_P (modulo π) with the help of an interferometric array by comparing two interferograms, one of them obtained for $\Phi_P = 0$, i.e., $U = I$, and serving us as a reference, and the second interferogram corresponding to the applied U. The relative shift of the latter with respect to the reference interferogram gives us Φ_P. Now, the unitary transformations that we can implement using common optical devices like quarter-wave plates (Q) and half-wave plates (H) are of the form

$$U(\xi,\eta,\zeta) = \exp\left(-i\frac{\xi}{2}\sigma_y\right)\exp\left(i\frac{\eta}{2}\sigma_z\right)\exp\left(-i\frac{\zeta}{2}\sigma_y\right). \tag{5}$$

They can be realized with the following gadget:

$$U(\xi,\eta,\zeta) = Q\left(\frac{-3\pi+2\xi}{4}\right)H\left(\frac{\xi-\eta-\zeta-\pi}{4}\right)Q\left(\frac{\pi-2\zeta}{4}\right). \tag{6}$$

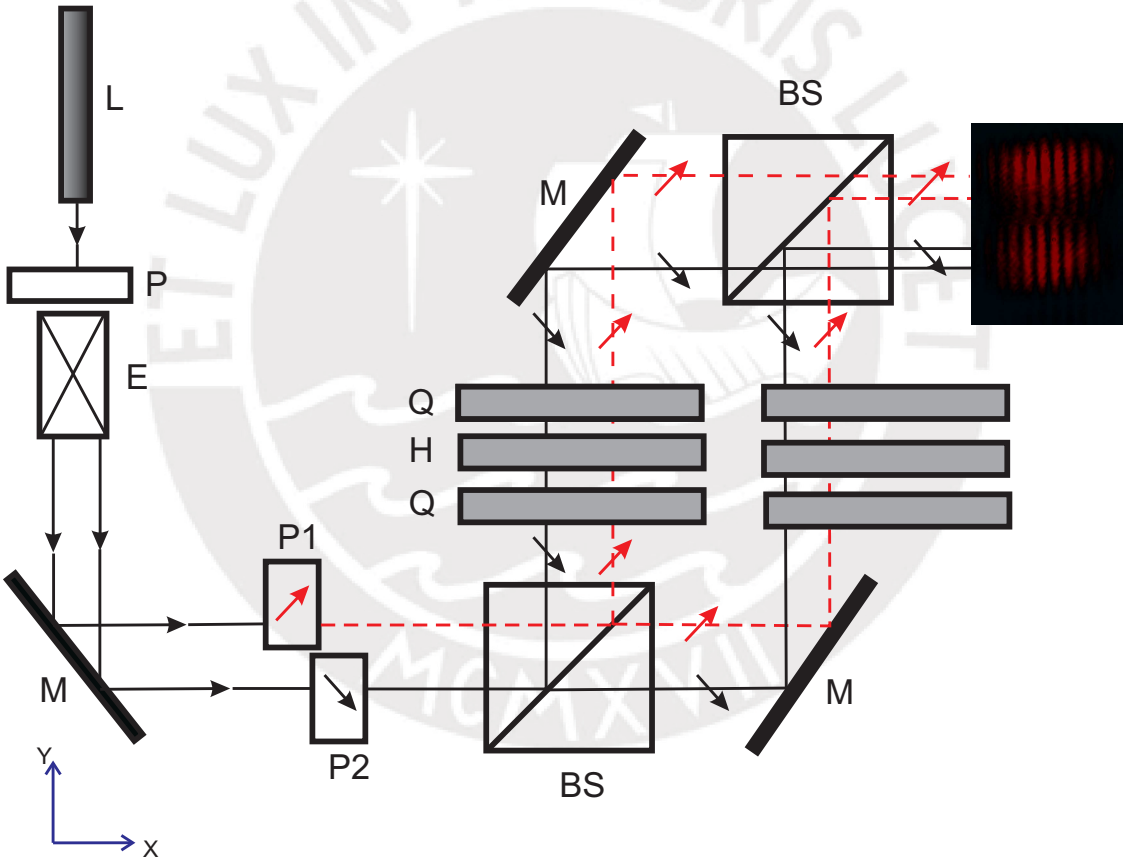

Figure 1. Interferometric setup for measuring the geometric phase (P: polarizer, BS: beam-splitter, M: mirror, E: beam expander, Q: $\lambda/4$ waveplate, H: $\lambda/2$ waveplate). The gadget QHQ on the left arm produces the desired unitary transformations, while that on the right arm nullifies the dynamic contribution to the total phase. Two interferograms are simultaneously produced and recorded. As the inset shows, one interferogram corresponds to the vertically polarized part, while the other corresponds to the horizontally polarized part of the expanded beam. From the relative shift between these interferograms one can obtain the geometric phase.

The corresponding interferogram has an intensity pattern given by

$$I_V = \left| \frac{1}{\sqrt{2}} \left(e^{i\phi} |+\rangle_z + U(\xi,\eta,\zeta) |+\rangle_z \right) \right|^2 = \tag{7}$$
$$= \frac{1}{2} \left[1 - \cos\left(\frac{\eta}{2}\right) \cos\left(\frac{\xi+\zeta}{2}\right) \cos(\phi) - \sin\left(\frac{\eta}{2}\right) \cos\left(\frac{\xi-\zeta}{2}\right) \sin(\phi) \right].$$

I_V refers to an initial state $|+\rangle_z$ that is vertically polarized. From the relationship connecting the two parametrizations, $U(\xi,\eta,\zeta)$ and $U(\beta,\gamma,\delta)$, of the same $U \in SU(2)$, one can show that I_V can also be written as

$$I_V = \frac{1}{2} \left[1 - \cos\beta \cos(\phi - \delta) \right]. \tag{8}$$

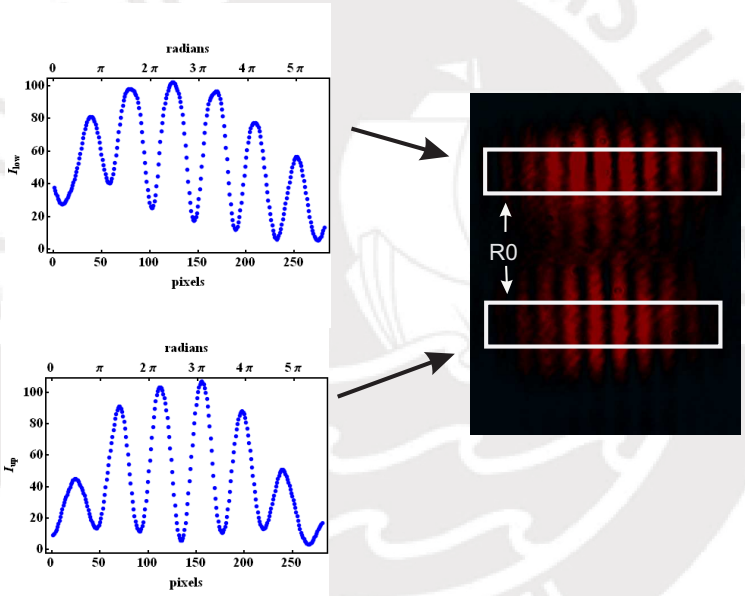

Figure 2. The geometric phase can be extracted from the relative fringe-shift between the upper and lower parts of the interferogram. The left panels show column averages of the fringes obtained after applying a low-pass filter to get rid of noise features. The column average is performed after selecting an evaluation area R_0, as illustrated on the right panel.

Pancharatnam's phase $\Phi_P = \delta$ is thus given by the shift of the interferogram whose intensity pattern is I_V, with respecto to a reference interferogram whose intensity pattern is $I = [1 - \cos\beta\cos\phi]/2$. By recording one interferogram after the other one could measure their relative shift. However, thermal and mechanical disturbances make it difficult to record stable reference patterns, thereby precluding accurate measurements of Φ_P. A way out of this situation follows from observing that the intensity pattern that corresponds to an initial, horizontally polarized state $|-\rangle_z$ is given by

$$I_H = \frac{1}{2} \left[1 - \cos(\beta) \cos(\phi + \delta) \right]. \tag{9}$$

Hence, the relative shift between I_V and I_H is just twice Pancharatnam's phase. This suggests dividing the laser beam into a vertically polarized part and a horizontally polarized part, something that can be achieved with the help of a beam-displacer prism. By so doing, we have the two parts of the laser beam being subjected to the same disturbances and we can record two interferograms in a single shot. The relative shift is thus easily measurable, being robust to thermal and mechanical disturbances. With such an array we were able to measure Pancharatnam's phase for different unitary transformations. Our results were reported in [1].

Our aim here is to measure a geometric phase Φ_g. Given a curve $\mathcal{C}_0$ in parameter space, Φ_g relates to Φ_P by

$$\Phi_g(C_0) = \Phi_P(\mathcal{C}_0) - \Phi_{dyn}(\mathcal{C}_0), \tag{10}$$

with

$$\Phi_P(\mathcal{C}_0) = \arg\langle\psi(s_1)|\psi(s_2)\rangle, \tag{11}$$

$$\Phi_{dyn}(\mathcal{C}_0) = \int_{s_1}^{s_2} Im\langle\psi(s)|\dot{\psi}(s)\rangle ds \tag{12}$$

While $\Phi_P(\mathcal{C}_0)$ and $\Phi_{dyn}(\mathcal{C}_0)$ depend on the curve $\mathcal{C}_0$ described by $|\psi(s)\rangle$ in parameter space, which in our case is the Poincaré sphere spanned by (θ, φ) in Eq.(1), $\Phi_g(C_0)$ turns out to depend only on the curve C_0 that is described by $|\psi(s)\rangle\langle\psi(s)|$. This object and hence also the curve C_0 are "gauge-invariant", i.e., invariant under parameter-dependent changes of the phase: $|\psi(s)\rangle \rightarrow \exp(i\alpha(s))|\psi(s)\rangle$. This is what makes $\Phi_g(C_0)$ a geometrical object. Exploiting such a gauge freedom we can choose an appropriate phase factor $\exp(i\alpha(s))$, so as to make $\Phi_{dyn}(\mathcal{C}_0) = 0$ along a given curve $\mathcal{C}_0 : |\psi(s)\rangle, s \in [s_1, s_2]$ which is traced out by our polarization states $|\psi(s)\rangle$ as a result of applying to an initial state $|\psi(0)\rangle$ some unitary transformation $U(s)$: $|\psi(s)\rangle = U(s)|\psi(0)\rangle$. Any $U(s)$ can be realized by making one or more of the parameters appearing in $U(\xi, \eta, \zeta)$ (see Eq.(6)) functions of s while keeping the other ones fixed. Hence, any desired curve on the Poincaré sphere can be realized in this way. Setting the corresponding QHQ-gadget on one arm of the interferometer we make the polarization state $|\psi(s)\rangle$ follow the prescribed curve. A second QHQ-gadget can be set on the other arm of the interferometer in order to produce with its help the factor $\exp(i\alpha(s))$ that is needed to nullify $\Phi_{dyn}(\mathcal{C}_0)$. This is achieved by observing that under the gauge transformation $|\psi(s)\rangle \rightarrow |\psi'(s)\rangle = \exp(i\alpha(s))|\psi(s)\rangle$ the integrand entering the definition of $\Phi_{dyn}(\mathcal{C}_0)$, Eq.(12), changes according to $Im\langle\psi(s)|\dot{\psi}(s)\rangle \longrightarrow Im\langle\psi'(s)|\dot{\psi}'(s)\rangle = Im\langle\psi(s)|\dot{\psi}(s)\rangle + \dot{\alpha}(s)$. Solving $Im\langle\psi(s)|\dot{\psi}(s)\rangle + \dot{\alpha}(s) = 0$ for $\alpha(s)$ we can fix the QHQ-gadget that makes $\Phi_{dyn}(\mathcal{C}_0) = 0$.

Our interferometric setup is shown in Fig.(1). It is of the Mach-Zehnder type; but a Sagnac-like and a Michelson-like interferometer could be used as well. With the help of this array we could measure geometric phases stemming from non-geodesic trajectories on the Poincaré sphere. Our results will be discussed in the next section.

3. Experimental results

We carried out our measurements employing a 30 mW, cw He-Ne laser (632.8 nm) to feed the interferometric array shown in Fig.(1). The interferograms were recorded with the help of a CCD camera ($1/4''$ Sony, video format of 640×480 pixels, frame rate adjusted to 30 fps) and digitized with a computer. The upper and lower halves of the interferograms showed a small relative shift stemming from surface irregularities and tiny misalignments. We used a first interferogram taken without phase-shifting ($U = I$) to gauge all the successive ones that correspond to transformations $U(\xi, \eta, \zeta) \neq I$. They were evaluated using an algorithm that

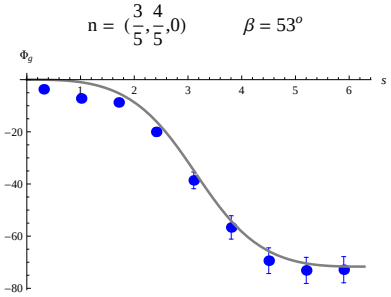

Figure 3. Geometric phase for a non-geodesic trajectory on the Poincaré sphere. The trajectory is a circle, which is the intersection of a cone with the Poincaré sphere. It is specified by giving n, the axis of the cone, and β, its aperture angle.

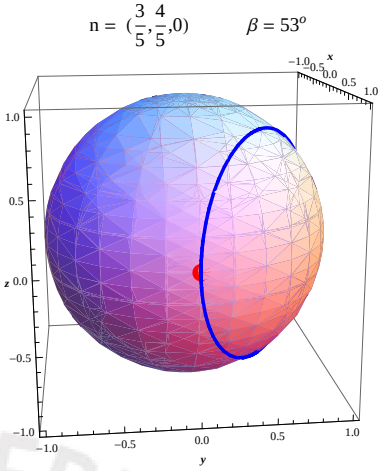

Figure 4. The trajectory described on the Poincaré sphere as the polarization is continuously changed with simultaneous cancelling of the dynamic contribution.

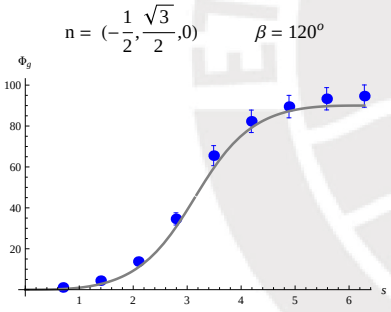

Figure 5. Geometric phase for a non-geodesic trajectory.

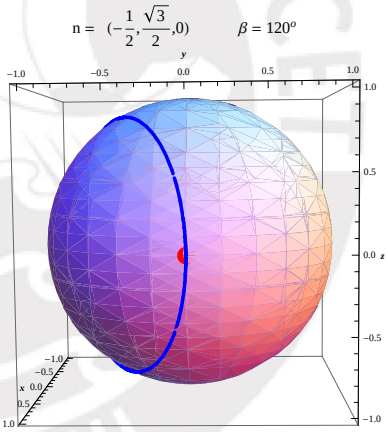

Figure 6. The trajectory on the Poincaré sphere.

works as follows. First, by optical inspection one selects (defining pixel numbers) a common region R_0 of the images that the algorithm should work with (see Fig. (1)). The algorithm performs a column average of each half of the interferogram and the output is then submitted to a low-pass filter to get rid of noisy features. For each pair of curves the algorithm searches for relative minima and compares their locations. It gives as a first output the relative shifts between the minima. After averaging these relative shifts the algorithm produces a final output for each pair of curves. We repeated this procedure for a series of regions: $R_0 \ldots R_3$, that were defined by their pixel numbers, in order to estimate the accuracy of our results. We applied this procedure to a whole set of interferograms corresponding to different choices of $U(\xi, \eta, \zeta)$. Our results are shown in Figs. (3) to (8). As can be seen, our experimental results are in very good agreement with theoretical predictions. As expected (retarders and polarizers could be oriented to within 1^0), the experimental values were within 6% in accordance with the theoretical predictions.

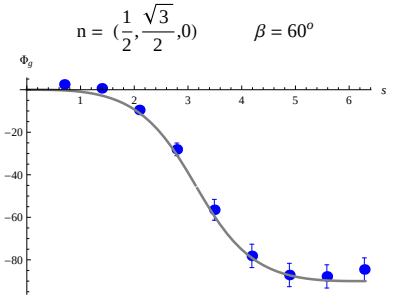

Figure 7. Geometric phase for a non-geodesic trajectory.

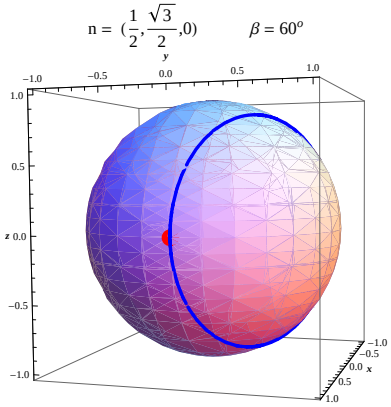

Figure 8. The trajectory on the Poincaré sphere.

4. Conclusions and outlook

We have implemented a robust interferometric array to measure geometric phases. Our setup allows producing and measuring geometric phases with great versatility, without the restriction of having to move polarization states along paths that are composed of geodesic segments. Given a path, we could submit the polarization state to a transformation that nullifies the dynamical contribution to its total (Pancharatnam) phase, so as to obtain a purely geometric phase. Our results represent a proof-of-principle that could be applied to different arrays. These arrays ought to be capable of implementing unitary transformations on two qubits that are carried along by a single beam, as it occurs in our case, where a laser beam was divided into two halves. One half was vertically, and the other half horizontally polarized. In this way one can get rid of the commonly encountered instabilities of interferometric arrays. The robustness of our setup is similar to the one achieved using a polarimetric approach. The results obtained by using the latter will be reported elsewhere.

As a next step, we plan to submit our polarization states to random disturbances in order to test the robustness of the geometric phase against decoherence. Thereafter, the single-photon version of our experiments should be implemented, in order to prove that the same array can be used to construct geometric quantum gates.

References

[1] Loredo J C, Ortíz O, Weingärtner R and De Zela F 2009 *Phys. Rev.* A **80** 0121113
[2] Pancharatnam S 1956 *Proc. Indian Acad. Sci.* A **44** 247
[3] Wagh A G and Rakhecha V C 1995 *Phys. Lett.* A **197** 112
[4] Ferrari J A and Frins E M 2002 *Appl. Opt.* **41**, 5313, Ferrari J A and Frins E M 2007 *Opt. Commun.* **279** 235
[5] Zanardi P and Rasetti M 1999 *Phys. Lett.* A **264** 94
[6] Jones J A, Vedral V, Ekert A and Castagnoli G 2000 *Nature* **403** 869
[7] Solinas P, Zanardi P, Zangh'i N and Rossi F 2003 *Phys. Rev.* B **67** 121307
[8] Duan L M, Cirac J I and Zoller P 2001 *Science* **292** 1695
[9] Ota Y, Goto Y, Kondo Y and Nakahara M 2009 *Phys. Rev.* A. **80** 052311
[10] Blais A and Tremblay A -M S 2003 *Phys. Rev.* A. **67** 012308

Measurement of Pancharatnam's phase by robust interferometric and polarimetric methods

J. C. Loredo,[1] O. Ortíz,[1] R. Weingärtner,[1,2] and F. De Zela[1]
[1]*Departamento de Ciencias, Sección Física, Pontificia Universidad Católica del Perú, Apartado, Lima 1761, Peru*
[2]*Department of Materials Science 6, University of Erlangen-Nürnberg, Martensstrasse 7, 91058 Erlangen, Germany*
(Received 17 April 2009; published 24 July 2009)

We report on theoretical calculations and experimental observations of Pancharatnam's phase originating from arbitrary SU(2) transformations applied to polarization states of light. We have implemented polarimetric and interferometric methods, which allow us to cover the full Poincaré sphere. As a distinctive feature, our interferometric array is robust against mechanical and thermal disturbances, showing that the polarimetric method is not inherently superior over the interferometric one, as previously assumed. Our strategy effectively amounts to feeding an interferometer with two copropagating beams that are orthogonally polarized with respect to each other. It can be applied to different types of standard arrays, such as a Michelson, a Sagnac, or a Mach-Zehnder interferometer. We exhibit the versatility of our arrangement by performing measurements of Pancharatnam's phases and fringe visibilities that closely fit the theoretical predictions. Our approach can be easily extended to deal with mixed states and to study decoherence effects.

DOI: 10.1103/PhysRevA.80.012113 PACS number(s): 03.65.Vf, 03.67.Lx, 42.65.Lm

I. INTRODUCTION

As is well known, Pancharatnam's phase was originally introduced to deal with the relative phase of two polarized light beams [1]. It anticipated geometrical phases that are nowadays intensively studied both theoretically and experimentally. Among all geometrical phases, Berry's phase [2] has played a major role in prompting the upsurge of a vast amount of investigations dealing with topological phases in quantum and classical physics. Berry's phase was originally introduced by considering the adiabatic evolution of a quantum state subjected to the action of a parameter-dependent Hamiltonian. However, the first experiments aiming at exhibiting such a phase were performed with classical states of light, using cw lasers [3]. It was soon realized that the phase tested in such experiments differed from Berry's phase, as it was larger than the latter by a factor of 2. The reason for this was that the experimentally studied phase [3] arose from SO(3) instead of SU(2) transformations. Indeed, Tomita and Chiao [3] let polarized light pass a coiled optical fiber and measured the phase originated from the adiabatic change suffered by the propagation direction of a light beam. Thus, the corresponding parameter space being explored—the sphere of directions—differed from the parameter space that was involved in Berry's original phase. The latter was Bloch sphere, on which any spin-1/2 state can be represented. Another two-state system formally equivalent to a spin-1/2 state is a polarized light, in which, e.g., vertically (V) and horizontally (H) polarized states constitute the counterparts of the spin-up and spin-down quantum states. Polarization states can be represented on the Poincaré sphere, which is equivalent to the Bloch sphere. An early experiment testing the appearance of Pancharatnam's phase in polarization states describing closed paths on the Poincaré sphere was the one performed by Bhandari and Samuel [4]. This interferometric test was however restricted to a limited set of SU(2) transformations and, moreover, some of the transformations used by the authors were nonunitary, as they employed linear polarizers to bring the polarization back to its initial value. Thus, Chyba *et al.* [5] performed alternative tests by employing only unitary transformations to exhibit Pancharatnam's phase, although such transformations were still restricted to cover a limited SU(2) range. In spite its original formulation in terms of polarization states of light, Pancharatnam's phase has not been fully exhibited in optical implementations, in contrast to more recent experiments based on neutron spin interferometry [6–8]. Some years ago, Wagh and Rakhecha [9,10] proposed two alternative methods to measure Pancharatnam's phase. One method is based on a polarimetric procedure, while the other is an interferometric one. Both procedures have been tested and compared against one another in experiments using neutrons [6,7]. The conclusion drawn from these experiments was that the polarimetric method is inherently superior over the interferometric method. This is so mainly because the polarimetric method is insensitive to mechanical and thermal disturbances that usually plague interferometric methods. Neutron interferometry, in particular, is also limited through spatial constraints that are imposed by the geometry of the monocrystals used to construct the interferometers. In order to explore a large range in the parameter space of the geometric phase, people contrived to realize some regions of this space by electrically inducing phase changes that were beyond the range accessible through rotation of a flipper. However, such a procedure prompted some criticisms [11] concerning the parameter spaces that were involved in the two phase evolutions, as one of them was physically obtained by the rotation of a flipper and the other by electrical means. On the other hand, the allegedly more accurate polarimetric method allows phase measurements only modulo π and is therefore unable to verify certain features such as the anticommutation of Pauli matrices, e.g., $\sigma_x\sigma_y=-\sigma_y\sigma_x$, which is something that was beautifully done with the interferometric method [6].

To the best of our knowledge, the two methods referred to above have not yet been tested against each other in all-optical experiments being capable of exploring the full parameter range of the Poincaré sphere. We have thus endeavored to compare both methods of measuring Pancharatnam's phase by using all-optical setups. In this work we present a

robust interferometric arrangement that makes the full range of SU(2) polarization transformations accessible. Furthermore, we have also implemented a polarimetric array with a similar coverage, so that both methods could be compared against each other. As we shall see, our interferometric arrangement is insensitive to mechanical and thermal disturbances. This represents an important improvement, as compared to conventional interferometric arrangements. The latter are usually set up as a variant of a Michelson, a Mach-Zehnder, or a Sagnac interferometer. Our method works with any of these variants, so that one could choose the most appropriate arrangement. For example, one could explore decoherence effects by measuring geometric phases in polarization single-photon mixed states using Mach-Zehnder interferometers, similarly to recently reported experiments [12]. In such a case, the fringe contrast (visibility) of the interferometric pattern also conveys information about the geometric phase. Although our work deals with pure states only, we have also tested the visibility of our patterns as a function of SU(2) transformations, obtaining very good agreement with theoretical predictions.

Our experiments, in addition to test Pancharatnam's phase with great versatility, serve the purpose of showing a common ground for classical and quantum manifestations of topological phases. Indeed, although our tests have been performed with classical states of light, they could be straightforwardly extended to experiments with single photons. Our theoretical discussion has thus been couched in a quantum-mechanical language, so that, e.g., the polarization states of classical light are represented by kets like $|V\rangle$ and $|H\rangle$. It should thus be clear that the features under study are not of an intrinsic classical or quantum-mechanical nature. Instead, it is the topological aspect that manifests itself as a common ground for both classical and quantum phenomena.

The paper is organized as follows. In Sec. II we review the interferometric and the polarimetric methods for measuring Pancharatnam's phase and derive theoretical results that apply in our case. In Sec. III we describe our experimental arrangements and present our results, comparing them with our theoretical predictions. Finally, we present in Sec. IV our conclusions.

II. INTERFEROMETRIC AND POLARIMETRIC METHODS

Given two states, $|i\rangle$ and $|f\rangle$, their Pancharatnam's relative phase Φ_P is defined as $\Phi_P=\arg\langle i|f\rangle$. A very direct way to exhibit Φ_P is through interferometry. Indeed, consider two interfering nonorthogonal states $|i\rangle$ and $|f\rangle$, with $|i\rangle \neq |f\rangle$. If we apply a phase shift ϕ to one of the states, the resulting intensity pattern is given by

$$I = |e^{i\phi}|i\rangle + |f\rangle|^2 = 2 + 2|\langle i|f\rangle|\cos(\phi - \arg\langle i|f\rangle). \quad (1)$$

The maxima of I are thus attained at $\phi=\arg\langle i|f\rangle=\Phi_P$. We are interested in exhibiting Φ_P in two-level systems and when Pancharatnam's phase arises as a consequence of having submitted an initial state $|i\rangle$ to an arbitrary transformation $U \in \mathrm{SU}(2)$ that converts it into a final state $|f\rangle=U|i\rangle$. The intensity measurement for which Eq. (1) applies can be implemented with the help of, say, a Mach-Zehnder interferometer. Alternatively, one could employ polarimetric methods. We will discuss both methods in what follows. But before, and for later reference, let us introduce the two parametrizations of $U \in \mathrm{SU}(2)$ that we shall use in our analysis. We call them the *YZY* and the *ZYZ* forms for obvious reasons: the first one is given by

$$U(\xi,\eta,\zeta) = \exp\left(-i\frac{\xi}{2}\sigma_y\right)\exp\left(i\frac{\eta}{2}\sigma_z\right)\exp\left(-i\frac{\zeta}{2}\sigma_y\right), \quad (2)$$

while the second form is given by

$$U(\beta,\gamma,\delta) = \exp\left[i\left(\frac{\delta+\gamma}{2}\right)\sigma_z\right]\exp(-i\beta\sigma_y)\exp\left[i\left(\frac{\delta-\gamma}{2}\right)\sigma_z\right]$$
$$= \begin{pmatrix} e^{i\delta}\cos\beta & -e^{i\gamma}\sin\beta \\ e^{-i\gamma}\sin\beta & e^{-i\delta}\cos\beta \end{pmatrix}. \quad (3)$$

To pass from one form of U to the other, one needs to connect the respective parameters. The corresponding equations of transformation involve, generally, trigonometric formulas, so that the different parameters are not connected to one another through algebraic relations [16]. The representation of Eq. (3) is particularly well adapted to exhibit Pancharatnam's phase. Indeed, taking as initial state $|i\rangle=|+\rangle_z$, i.e., the eigenstate of σ_z that belongs to the eigenvalue of +1, and setting $|f\rangle=U|+\rangle_z$ we have

$$\langle i|f\rangle = {}_z\langle +|U(\beta,\gamma,\delta)|+\rangle_z = e^{i\delta}\cos\beta. \quad (4)$$

From the definition of Pancharatnam's phase, i.e., $\Phi_P=\arg\langle i|f\rangle$, we obtain $\Phi_P=\delta+\arg(\cos\beta)$, for $\beta\neq(2n+1)\pi/2$. Because $\cos\beta$ can take on positive and negative real values, $\arg(\cos\beta)$ equals 0 or π. Hence, Φ_P is defined modulo π. In any case, the parametrization $U(\beta,\gamma,\delta)$ of Eq. (3) is seen to be most appropriate to exhibit $\Phi_P=\delta$ (modulo π). On the other hand, for the optical implementation of U, the parametrization of the *YZY* form is more appropriate. Indeed, it is well known [13] that with the help of three retarders, viz., two quarter-wave plates and one half-wave plate, it is possible to implement any $U \in \mathrm{SU}(2)$ in the polarization space of, e.g., horizontally and vertically polarized states of light: $\{|H\rangle,|V\rangle\}$. This requires that one represents U in the form given by Eq. (2), i.e., the *YZY* form, because of the following relationship involving the Euler angles $\theta_1,\theta_2,\theta_3$ (see, e.g., [14]):

$$\exp[-i(\theta_3+3\pi/4)\sigma_y]\exp[i(\theta_1-2\theta_2+\theta_3)\sigma_z]$$
$$\times\exp[i(\theta_1-\pi/4)\sigma_y] = Q(\theta_3)H(\theta_2)Q(\theta_1). \quad (5)$$

Here, Q means a quarter-wave plate and H means a half-wave plate. The arguments of the retarders are the angles of their major axes to the vertical direction. In the case of a U given by Eq. (2), by applying Eq. (5) we obtain

$$U(\xi,\eta,\zeta) = Q\left(\frac{-3\pi+2\xi}{4}\right)H\left(\frac{\xi-\eta-\zeta-\pi}{4}\right)Q\left(\frac{\pi-2\zeta}{4}\right). \quad (6)$$

Having discussed the two parametrizations of $U \in \mathrm{SU}(2)$ that are useful for our purposes, we turn now to the implementa-

tion of the experimental arrangements that allow us to exhibit Pancharatnam's phase.

A. Interferometric arrangement: Mach-Zehnder and Sagnac

In general, with an interferometric array Pancharatnam's phase can be drawn from intensity measurements that are essentially described by Eq. (1). If we introduce U as given in Eq. (2) into Eq. (1), we obtain the intensity as

$$I = \left| \frac{1}{\sqrt{2}}[e^{i\phi}|+\rangle_z + U(\xi,\eta,\zeta)|+\rangle_z] \right|^2$$
$$= 1 - \cos\left(\frac{\eta}{2}\right)\cos\left(\frac{\xi+\zeta}{2}\right)\cos(\phi)$$
$$- \sin\left(\frac{\eta}{2}\right)\cos\left(\frac{\xi-\zeta}{2}\right)\sin(\phi). \quad (7)$$

From Eqs. (2) and (3) it follows that the parameters of these two representations of $U \in \mathrm{SU}(2)$ are related through $\tan(\delta)=\tan(\frac{\eta}{2})\cos(\frac{\xi-\zeta}{2})/\cos(\frac{\xi+\zeta}{2})$. Hence, I can be written as

$$I = 1 - \cos\left(\frac{\eta}{2}\right)\cos\left(\frac{\xi+\zeta}{2}\right)\sec(\delta)\cos(\delta-\phi), \quad (8)$$

making it evident that an interferometric method for exhibiting Φ_P would require measuring the shift induced by U on the intensity pattern by an angle $\delta=\Phi_P$ (modulo π). Now, the expression for I as given in Eq. (8) is somewhat inconvenient, because it mixes δ with parameters of a representation to which it does not belong. By expressing Eq. (8) with the parameters of $U(\beta,\gamma,\delta)$, we obtain

$$I = 1 - \cos(\beta)\cos(\delta-\phi), \quad (9)$$

thus rendering clear that the visibility $v \equiv (I_{\max}-I_{\min})/(I_{\max}+I_{\min})$ is given by $v=\cos\beta$, i.e., it is independent of Pancharatnam's phase. In terms of the parameters ξ,η,ζ the square of the visibility is given by

$$v^2(\xi,\eta,\zeta) = \tfrac{1}{2}[1+\cos\xi\cos\zeta-\cos\eta\sin\xi\sin\zeta]. \quad (10)$$

For experimental tests, it will be useful to write the visibility in terms of the angles of the retarders as follows:

$$v^2(\theta_1,\theta_2,\theta_3) = \frac{1}{2}\left[1+\cos\left(\frac{3\pi+4\theta_3}{2}\right)\cos\left(\frac{\pi-4\theta_1}{2}\right)\right.$$
$$-\cos(2\theta_1-4\theta_2+2\theta_3)$$
$$\left.\times\sin\left(\frac{3\pi+4\theta_3}{2}\right)\sin\left(\frac{\pi-4\theta_1}{2}\right)\right]. \quad (11)$$

Let us now refer specifically to a Mach-Zehnder interferometer. In order to calculate its output intensity, let us represent light beams as a superposition of polarization states ($\{|H\rangle,|V\rangle\}$) and momentum (or "which way," i.e., spatial) states ($\{|X\rangle,|Y\rangle\}$). These last states denote the two-way alternative that can be ascribed to the Mach-Zehnder interferometer. Let us consider first that our initial state is taken to be a vertically polarized state that enters the first beam splitter along the X direction (e.g., the beam passing polarizer P_1 in Fig. 1). It is represented by $|VX\rangle \equiv |V\rangle\otimes|X\rangle$. The actions of beam splitters, mirrors, and phase shifters are represented by operators in the two-qubit space with basis $\{|VX\rangle,|VY\rangle,|HX\rangle,|HY\rangle\}$. They act on the $|X\rangle,|Y\rangle$ states, leaving the polarization states $|H\rangle,|V\rangle$ unchanged. The actions of a 50:50 beam splitter and a mirror are given, respectively, by [14]

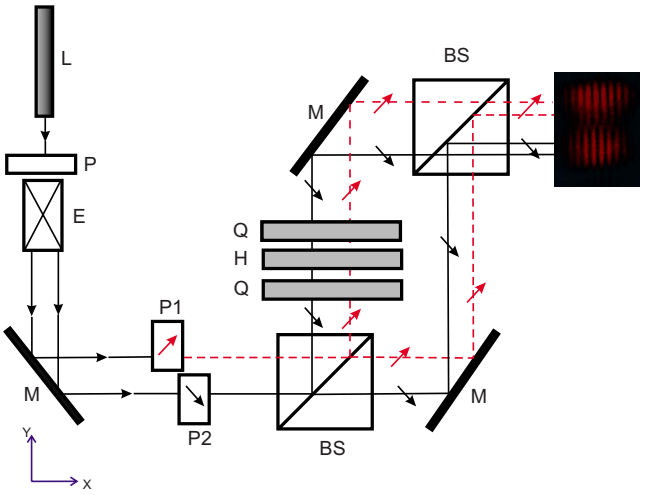

FIG. 1. (Color online) Interferometric arrangement for testing Pancharatnam's phase Φ_P. Light from a He-Ne laser (L) passes a polarizer (P) and enters a beam expander (E), after which half of the beam goes through one polarizer (P_1) and the other half goes through a second polarizer (P_2), orthogonally oriented with respect to the first. The two collinear beams feed the same Mach-Zehnder interferometer (BS: beam splitter; M: mirror) in one of whose arms an array of three retarders has been mounted (Q:quarter-wave plate; H: half-wave plate), so as to realize any desired SU(2) transformation. This transformation introduces a Pancharatnam's phase $\Phi_P=\delta$ on one half of the beam and an opposite phase $\Phi_P=-\delta$ on the other perpendicularly polarized half, so that the relative phase of the two halves equals 2δ. From the relative shift between the upper and the lower halves of the interferogram that is captured by a CCD camera set at the output of the array, one can determine Φ_P. Any instability of the array affects both halves of the interferogram in the same way, so that the relative shift of 2δ is insensitive to instabilities.

$$U_{BS} = 1_P \otimes \frac{1}{\sqrt{2}}(|X\rangle\langle X| + |Y\rangle\langle Y| + i|X\rangle\langle Y| + i|Y\rangle\langle X|), \quad (12)$$

$$U_{mirr} = 1_P \otimes [-i(|X\rangle\langle Y| + |Y\rangle\langle X|)], \quad (13)$$

where 1_P means the identity operator in polarization space. Let us stress that the above expressions for the actions of a beam splitter and a mirror hold true irrespective of the fact that the spatial qubits are realized by classical or by quantum fields (see, e.g., [15]). Working with classical fields, the usage of kets (and bras) is just a useful mathematical means to represent field amplitudes [16]. Accordingly, a phase factor in one or in the other arm of the interferometer can be represented by $U_X(\phi)=1_P\otimes(\exp(i\phi)|X\rangle\langle X|+|Y\rangle\langle Y|)$ and $U_Y(\phi)=1_P\otimes(|X\rangle\langle X|+\exp(i\phi)|Y\rangle\langle Y|)$, respectively. If we mount an

array of retarders on, say, arm X of the interferometer, its action would be represented by $U_P^X = U \otimes |X\rangle\langle X| + 1_P \otimes |Y\rangle\langle Y|$, where $U \in \mathrm{SU}(2)$ means the respective polarization transformation that the retarders produce, in our case the one given in Eq. (2). Similarly, $U_P^Y = 1_P \otimes |X\rangle\langle X| + U \otimes |Y\rangle\langle Y|$. For the arrangement shown in Fig. 1 we obtain

$$U_T = U_{BS} U_{mirr} U_X(\phi) U_P^Y U_{BS}. \tag{14}$$

This U acts on the initial state $|VX\rangle$ and the intensity measured at one of the output ports of the final beam splitter is obtained by projecting the resulting state, $U_T|VX\rangle$, with the appropriate projectors: $|VX\rangle\langle VX|$ and $|HX\rangle\langle HX|$, thereby obtaining the vectors $|VX\rangle\langle VX|U_T|VX\rangle$ and $|HX\rangle\langle HX|U_T|VX\rangle$, respectively. Squaring the respective amplitudes and summing up we get the intensity as $I_V = |\langle VX|U_T|VX\rangle|^2 + |\langle HX|U_T|VX\rangle|^2$. A straightforward calculation yields

$$I_V = \frac{1}{2}\left[1 - \cos\left(\frac{\eta}{2}\right)\cos\left(\frac{\xi+\zeta}{2}\right)\cos(\phi) - \sin\left(\frac{\eta}{2}\right)\cos\left(\frac{\xi-\zeta}{2}\right)\sin(\phi)\right]. \tag{15}$$

As already shown, this can be written as

$$I_V = \tfrac{1}{2}[1 - \cos(\beta)\cos(\phi - \delta)]. \tag{16}$$

Using the above result, a direct measurement of Pancharatnam's phase $\delta = \Phi_P$ (modulo π) becomes possible: all one needs to do is to measure the fringe shift between two interferograms, with one of them serving as the reference ($\delta = 0$) and the other being obtained after applying the U transformation. The practical problem with this method is the instability of the interferometric array. Minute changes in any component of the interferometer preclude an accurate determination of δ. Different strategies can be applied to overcome this kind of shortcomings. Mechanical and thermal isolations of the arrangement is the most direct one, but it makes measurements rather awkward. Damping instabilities by a feedback mechanism is another possibility; but it makes the arrangement more involved and difficult to operate. A third option would be to use a Sagnac instead of a Mach-Zehnder interferometer. In a Sagnac-like interferometer one can make the two beams pass the same optical elements, so that any instability would affect both beams equally. One should then design the interferometer in such a way that the U transformation acts on one beam alone, so that the other can serve as the reference beam. In our case, for reasons explained in detail in Sec. III, we turned to a different option that is based on the following observations.

Equation (16) holds for an initial state that is vertically polarized. When the initial state is horizontally polarized, then the intensity is given by

$$I_H = \tfrac{1}{2}[1 - \cos(\beta)\cos(\phi + \delta)]. \tag{17}$$

We observe that intensities I_V and I_H are shifted with respect to each other by 2δ. Thus, we can exploit this fact for measuring δ. To this end, we polarize one half—say the upper half—of the laser beam vertically and the lower half horizontally. With such a beam we feed our interferometer. It can be mounted either in a Mach-Zehnder or in a Sagnac configuration. In both cases we can capture at the output an interferogram, half of which corresponds to I_V and the other half corresponds to I_H. The upper fringes of the output will be shifted with respect to the lower ones by 2δ. As both halves of the beam pass the same optical elements, they will be equally affected by whatever perturbations. The array is therefore insensitive to instabilities. We thus need only to accurately measure the relative fringe shift in each interferogram in order to obtain δ. By applying this method, we have measured Pancharatnam's phase with an accuracy that is similar to that reached by the polarimetric method, on which we turn next.

B. Polarimetric arrangement

The optical setup for the polarimetric method, as proposed by Wagh and Rakhecha [9], is somewhat more demanding as compared to the interferometric method. At first sight, however, the polarimetric method could appear to be the simpler of the two options, because it requires a single beam, from which one extracts phase information. It is not obvious that phase information can be extracted from a single beam. However, the polarimetric method is in fact based on an analogous principle as the interferometric one, and in a certain sense polarimetry could be seen as "virtual interferometry." Let us briefly discuss how it works.

Consider an initial polarized state $|i\rangle = |+\rangle_z$ and submit it to the action of a $\pi/2$ rotation around an axis perpendicular to the polarization axis (z), e.g., a rotation around the x axis. As a result, we obtain the state $(|+\rangle_z - i|-\rangle_z)/\sqrt{2}$. If we now phase shift this state by applying to it the operator $\exp(-\phi\sigma_z/2)$, we obtain the state

$$\begin{aligned} V|+\rangle_z &\equiv \exp(-i\phi\sigma_z/2)\exp(-i\pi\sigma_x/4)|+\rangle_z \\ &= (e^{-i\phi/2}|+\rangle_z - ie^{i\phi/2}|-\rangle_z)/\sqrt{2} \\ &= e^{-i\phi/2}(|+\rangle_z - ie^{i\phi}|-\rangle_z)/\sqrt{2}. \end{aligned}$$

We have thus generated a relative phase ϕ between the states $|+\rangle_z$ and $|-\rangle_z$, which is something analogous to what is achieved in an interferometer by changing the length of one of the two optical paths. Subsequently, we let U act and as a result we obtain the state $UV|+\rangle_z = (e^{-i\phi/2}U|+\rangle_z - ie^{i\phi/2}U|-\rangle_z)/\sqrt{2} \equiv |\chi_+\rangle + |\chi_-\rangle$. It is from this last state that we can extract Pancharatnam's phase by intensity measurements. In order to accomplish this goal, we project $|\chi_+\rangle + |\chi_-\rangle$ on the state $V|+\rangle_z$, i.e., the phase-shifted split state we prepared before applying U. The corresponding intensity we measure is thus given by

$$I = |{}_z\langle + |V^\dagger(|\chi_+\rangle + |\chi_-\rangle)|^2. \tag{18}$$

Let us write $V|+\rangle_z = (e^{-i\phi/2}|+\rangle_z - ie^{i\phi/2}|-\rangle_z)/\sqrt{2} \equiv |\varphi_+\rangle + |\varphi_+\rangle$ and take U as given by $U(\beta, \gamma, \delta)$ of Eq. (3). Calculating the amplitude ${}_z\langle +|V^\dagger(|\chi_+\rangle + |\chi_-\rangle) = (\langle\varphi_+| + \langle\varphi_-|)(|\chi_+\rangle + |\chi_-\rangle)$, we obtain, using $\langle\varphi_\pm|\chi_\pm\rangle = \exp(\pm i\delta)\cos(\beta)/2$ and $\langle\varphi_\mp|\chi_\pm\rangle = i\exp[\mp i(\gamma+\phi)]\sin(\beta)/2$, that $(\langle\varphi_+| + \langle\varphi_-|)(|\chi_+\rangle + |\chi_-\rangle) = \cos(\beta)\cos(\delta) + i\sin(\beta)\cos(\gamma+\phi)$ and, hence, that the intensity amounts to

$$I = \cos^2(\beta)\cos^2(\delta) + \sin^2(\beta)\cos^2(\gamma + \phi). \tag{19}$$

Equation (19) contains Pancharatnam's phase $\delta=\Phi_P$ (modulo π) in a form that allows its extraction through intensity measurements. Indeed, we observe from Eq. (19) that the minimal and the maximal intensities are given by $I_{\min}=\cos^2(\beta)\cos^2(\delta)$ and $I_{\max}=\cos^2(\beta)\cos^2(\delta)+\sin^2(\beta)$, respectively, so that

$$\cos^2(\delta)=\frac{I_{\min}}{1-I_{\max}+I_{\min}}, \tag{20}$$

which is the expression on which the polarimetric method is finally based.

A concrete experimental arrangement requires that we implement V and U with the help of retarders. To begin with, $\exp(-i\pi\sigma_x/4)=Q(\frac{\pi}{4})$ and $\exp(-i\phi\sigma_z/2)=Q(\frac{\pi}{4})H(\frac{\phi-\pi}{4})Q(\frac{\pi}{4})$. Using $Q^2(\frac{\pi}{4})=H(\frac{\pi}{4})$ and $\exp(+i\phi\sigma_z/2)=Q(-\frac{\pi}{4})H(\frac{\phi+\pi}{4})\times Q(-\frac{\pi}{4})$, we obtain

$$\begin{aligned}U_{tot}&\equiv V^{\dagger}UV\\&=H\left(-\frac{\pi}{4}\right)H\left(\frac{\phi+\pi}{4}\right)Q\left(-\frac{\pi}{4}\right)\\&\quad\times UQ\left(\frac{\pi}{4}\right)H\left(\frac{\phi-\pi}{4}\right)H\left(\frac{\pi}{4}\right).\end{aligned} \tag{21}$$

As for U, it is convenient to employ the form $U(\xi,\eta,\zeta)$ of Eq. (2), a form which can be directly translated into an arrangement with retarders, according to Eq. (6), i.e., an arrangement of the form QHQ. Inserting this QHQ for U into Eq. (21), we end up with an arrangement that consists of nine plates. In order to reduce the number of plates, we apply relations such as, e.g., $Q(\alpha)H(\beta)=H(\beta)Q(2\beta-\alpha)$, $Q(\alpha)H(\beta)H(\gamma)=Q(\alpha+\pi/2)H(\alpha-\beta+\gamma-\pi/2)$. The final reduction gives an array that consists of five retarders:

$$\begin{aligned}U_{tot}&=Q\left(-\frac{3\pi}{4}-\frac{\phi}{2}\right)Q\left(-\frac{5\pi+2\xi}{4}-\frac{\phi}{2}\right)\\&\quad\times Q\left(-\frac{9\pi+2(\xi+\eta)}{4}-\frac{\phi}{2}\right)H\left(-\frac{7\pi+\xi+\eta-\zeta}{4}-\frac{\phi}{2}\right)\\&\quad\times Q\left(-\frac{\pi}{4}-\frac{\phi}{2}\right).\end{aligned} \tag{22}$$

Note that such an arrangement could be implemented by mounting five plates having a common rotation axis, so that all the plates can be rotated simultaneously by the same angle $\phi/2$. The intensity that we should measure at the detector depends on ξ, η, and ζ according to the following expression:

$$\begin{aligned}I&=|\langle_z+|U_{tot}|+\rangle_z|^2\\&=\cos^2\left(\frac{\eta}{2}\right)\cos^2\left(\frac{\xi+\zeta}{2}\right)\\&\quad+\left[\cos\left(\frac{\eta}{2}\right)\sin\left(\frac{\xi+\zeta}{2}\right)\cos(\phi)\right.\\&\quad\left.+\sin\left(\frac{\eta}{2}\right)\sin\left(\frac{\xi-\zeta}{2}\right)\sin(\phi)\right]^2.\end{aligned} \tag{23}$$

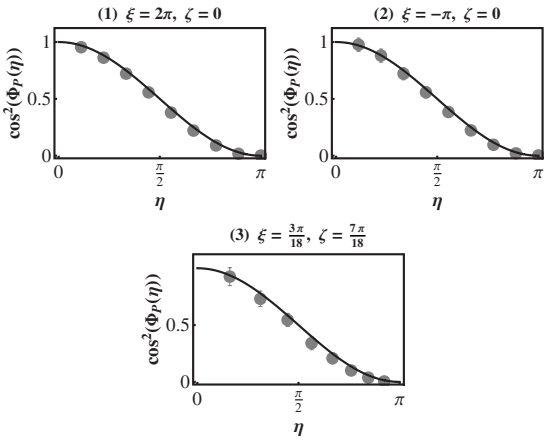

FIG. 2. Experimental results from a polarimetric measurement of Pancharatnam's phase. The upper graphs correspond to an array that consists of three retarders set in the forms QQH (left) and QHQ (right). Parameter values are as indicated and $\cos^2(\Phi_P)$ was measured as a function of η. The lower curve corresponds to the full array of five retarders set in the form $QQQHQ$.

From this intensity we can extract Pancharatnam's phase, as given by Eq. (20). We have tested this theoretical prediction under restricted conditions by manually rotating the retarders. Thus, we fixed ζ to 2π, so that $\cos^2(\delta)=I_{\min}(1-I_{\max}+I_{\min})^{-1}=\cos^2(\eta/2)$ for all ξ. In such a case, Pancharatnam's phase (modulo π) should be given by $\Phi_P=\eta/2$. For $\zeta=2\pi$ the arrangement that realizes the corresponding U_{tot} reduces to the following expression:

$$U_{tot}^{\xi=2\pi}=Q(\phi)Q\left(-\frac{\xi}{2}+\phi\right)H\left(\frac{\eta-\xi}{4}+\phi\right), \tag{24}$$

in which we have redefined the rotation angle ϕ according to $(-3\pi-2\phi)/4\rightarrow\phi$. If we instead fix $\xi=-\pi$, it still remains true that $\cos^2(\delta)=I_{\min}(1-I_{\max}+I_{\min})^{-1}=\cos^2(\eta/2)$, this time for all ζ, so that $\Phi_P=\eta/2$ (modulo π) as before. The corresponding arrangement of retarders is now given by

$$\begin{aligned}U_{tot}^{\xi=-\pi}&=Q\left(\frac{3\pi+2\eta-2\phi}{4}\right)H\left(\frac{-4\pi+\zeta+\eta-2\phi}{4}\right)\\&\quad\times Q\left(\frac{-\pi-2\phi}{4}\right).\end{aligned} \tag{25}$$

It is worth noting that the intensity in this case is given by

$$I=\cos^2\left(\frac{\zeta}{2}\right)\cos^2\left(\frac{\eta-2\phi}{2}\right)+\sin^2\left(\frac{\zeta}{2}\right)\cos^2\left(\frac{\eta}{2}\right). \tag{26}$$

Setting $\eta=0$, $\zeta=\pi$, the intensity has a constant value, which is useful for adjusting the arrangement. The results of our measurements, including those corresponding to the full array with five retarders, are shown in Fig. 2. As one can see, they confirm the theoretical predictions within experimental errors.

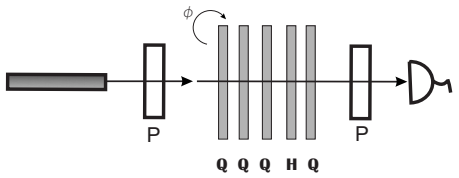

FIG. 3. Polarimetric arrangement for testing Pancharatnam's phase Φ_P. With an array of five retarders (Q:quarter-wave plate; H: half-wave plate) and two polarizers (P), a relative phase ϕ between two polarization components $|\pm\rangle_z$ can be introduced, on which any desired SU(2) transformation can be applied. The five retarders are simultaneously rotated, thereby varying ϕ, and the intensity $I(\phi)$ is recorded. From the maximum and the minimum values of I one can determine Φ_P, according to $\cos^2(\Phi_P)=I_{\min}/(1-I_{\max}+I_{\min})$.

III. EXPERIMENTAL PROCEDURES AND RESULTS

A. Polarimetric measurements

We have carried out measurements of the Pancharatnam phase by applying the polarimetric and the interferometric methods presented in the previous sections. In both cases the light source was a 30 mW cw He-Ne laser (632.8 nm). The polarimetric arrangement shown in Fig. 3 could have been designed so that the five retarders [see Eq. (22)] could be simultaneously rotated by the same amount. If one aims at systematically measuring Pancharatnam's phase with the polarimetric method, this would require having a custom-made apparatus on which one can mount the five plates with any desired initial orientation and then submit the whole assembly to rotation. As our aim was to simply exhibit the versatility of the method and to compare its accuracy with that of the interferometric method, we mounted a simple array of five independent retarders, so that each one of them could be manually rotated. With such an approach it takes some hours of painstaking manipulation to record all necessary data, whenever the experiment is performed with the full array of five retarders. For this reason, we initially restricted our tests to three retarders. This could be achieved by lowering the degrees of freedom, i.e., by fixing one of the three Euler angles, as explained in the previous section [see Eqs. (24) and (25)]. Having made measurements with three plates, we performed an additional run of measurements with the full arrangement of five retarders. Our results are shown in Fig. 2. They correspond to intensity measurements obtained with a high-sensitivity light sensor (Pasco CI-6604, Si PIN photodiode with spectral response in the range 320–1100 nm). As expected (retarders and polarizers could be oriented to within 1^0), the experimental values are within 3–6 % in accordance with the theoretical predictions, depending on the number of retarders being employed.

B. Interferometric measurements

We used two interferometric arrangements. One of them was a Mach-Zehnder interferometer and the other was a Sagnac interferometer. We started by mounting both interferometers in the standard way, but adding an array of three retarders on one arm for implementing any desired $U \in \mathrm{SU}(2)$. Usually, phase shifts ϕ, as appearing in Eq. (9), originate from moving one mirror with, e.g., a low-voltage piezotransducer. One can then record the interference pattern by sensing the light intensity with a photodiode set at one of the output ports of the exiting beam splitter. Alternatively, one can capture the whole interference pattern with a charge-coupled device (CCD) camera. The Mach-Zehnder interferometer is easier to mount in comparison to the Sagnac interferometer. However, it has the disadvantage of being more unstable against environmental disturbances, thus requiring the application of some stabilizing technique such as, e.g., a feedback system. In contrast, the Sagnac interferometer is very stable with respect to mechanical and thermal disturbances. Nevertheless, mounting a Sagnac interferometer can be difficult for geometrical reasons. By using one or the other method, one can obtain two interferograms—one with and the other without the retarders in place. In our case, capturing the whole interference pattern with a CCD camera—instead of sensing it with a photodiode—proved to be the most convenient approach with both arrangements, Mach-Zehnder and Sagnac. When working with the Mach-Zehnder array, we first implemented a feedback system in order to stabilize the reference pattern. One of the two paths followed by the laser beam was used for feedback. The feedback system should allow us to compensate the jitter and thermal drifts of the fringe patterns that preclude a proper measurement of the phase shift. This requires an electronic signal, after proportional-integral amplification, to be fed to a piezotransducer in a servoloop, so as to stabilize the interferometer, thereby locking the fringe pattern. Although we succeeded in locking the fringe pattern, the geometry of our array severely limited the parameter range we could explore. We thus turned to a different option, i.e., the one based on Eqs. (16) and (17). It required polarizing one half of the laser beam in one direction and the other half in a direction perpendicular to the first one.

In order to exhibit the feasibility of our interferometric method, we performed experiments with both Mach-Zehnder and Sagnac arrays. In both cases we obtained similar preliminary results. However, the systematic recording of our results corresponds to the Mach-Zehnder array shown in Fig. 1, as it was the simpler one to mount and manipulate. As shown in the figure, the initially polarized laser beam was expanded, so that its upper half passed through one polarizer P_1 and its lower half through a second polarizer P_2 orthogonally oriented with respect to the first. Each run started by setting the retarders so as to afford the identity transformation $Q(\pi/4)H(-\pi/4)Q(\pi/4)=1_P$; the corresponding interferogram was captured with a CCD camera (1/4″ Sony CCD, video format of 640×480 pixels, and frame rate adjusted to 30 fps) and digitized with an *IBM*-compatible computer. The upper and the lower halves of this interferogram showed a small relative shift stemming from surface irregularities and tiny misalignments. The initial interferogram served to gauge all the successive ones that correspond to transformations $U(\xi,\eta,\zeta)\neq 1_P$. Each interferogram was evaluated with the help of an algorithm that works as follows. First, by optical inspection of the whole set of interferograms—corresponding to a given $U(\xi,\eta,\zeta)$—one selects (by pixel numbers) a common region R_0 of the images the algorithm should work with (see Fig. 4). Having this region as its input

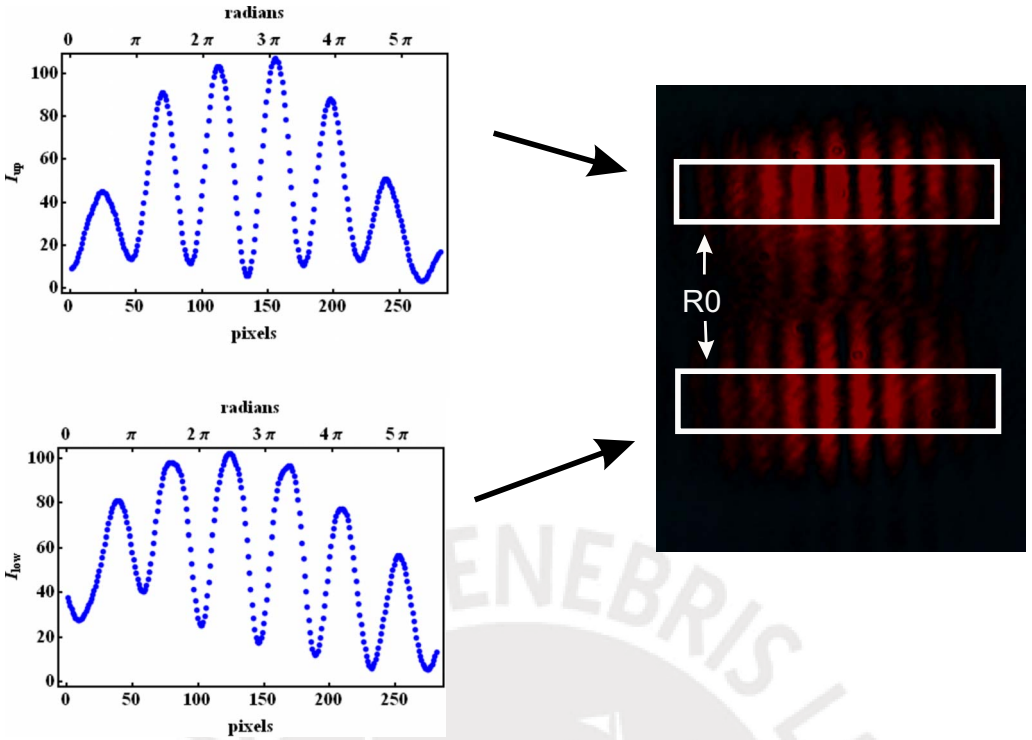

FIG. 4. (Color online) Pancharatnam's phase can be extracted from the relative fringe shift between the upper and the lower parts of the interferogram. The relative shift equals twice the Pancharatnam's phase. The left panels show the result of performing a column average of the fringes plus the application of a Savitzky-Golay filter to get rid of noise features. The column average is performed after selecting the evaluation area R_0 on the interferogram, as illustrated on the right panel. The reported shifts are mean values obtained from four different selections $R_0,\ldots,R_3$ of the evaluation area.

the algorithm performs a column average of each half of the interferogram—thereby obtaining the mean profile of the fringes—and the output is then submitted to a low-pass filter (Savitzky-Golay filter) to get rid of noisy features. The result is a pair of curves like those shown in Fig. 4. The algorithm then searches for relative minima in each of the two curves and compares their locations so as to output the relative shifts between the minima of the curves. After averaging these relative shifts the algorithm produces its final output for each pair of curves. We repeated this procedure for a series of regions (fixed by pixel numbers) $R_0,\ldots,R_3$, so that we could estimate the uncertainty of our experimental values. No attempt was made to automate the selection of the working regions. Visual inspection proved to be effective enough for our present purposes. Some series of interferograms showed limited regions that were clearly inappropriate for being submitted to evaluation, as they reflected inhomogeneities and other features that stemmed from surface irregularities of the optical components. We applied the complete procedure to a whole set of interferograms corresponding to different choices of $U(\xi,\eta,\zeta)$. Our results are shown in Fig. 5. As can be seen, our experimental results are in very good agreement with theoretical predictions.

A second independent, algorithm was also used to check the above results. This algorithm was developed as a variant of some commonly used procedures in image processing. Like in the previous approach, the algorithm first constructs the mean profiles of the fringes and submits them to a low-pass filter. But now, instead of searching for relative minima, the algorithm does the following. First, it determines the dominant spatial carrier frequency k_0 by Fourier transforming curves like those shown in Fig. 4. Let us denote these curves by $\hat{i}_{up}(x)$ and $\hat{i}_{low}(x)$, corresponding, respectively, to the upper and the lower halves of the interferogram. The Fourier transforms are denoted by $i_{up}(k)$ and $i_{low}(k)$. The goal is to determine the relative shift $\Delta_r=2\delta$ between $\hat{i}_{up}(x)$ and $\hat{i}_{low}(x)$. It can be shown [17] that $\Delta_r=\Delta_{up}-\Delta_{low}$

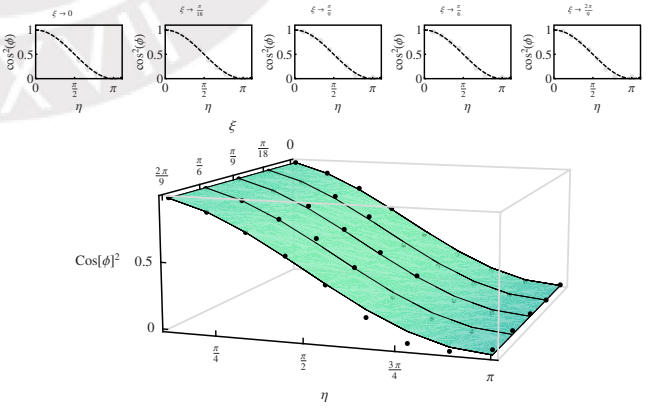

FIG. 5. (Color online) Experimental results from the interferometric measurement of Pancharatnam's phase. We plot $\cos^2(\Phi_P)$ as a function of ξ and η, with ζ being held fixed to zero. In the upper panels we plot the single curves that are highlighted on the surface shown on the lower panel. Dots correspond to experimental values, some of which fall below and some fall above the surface.

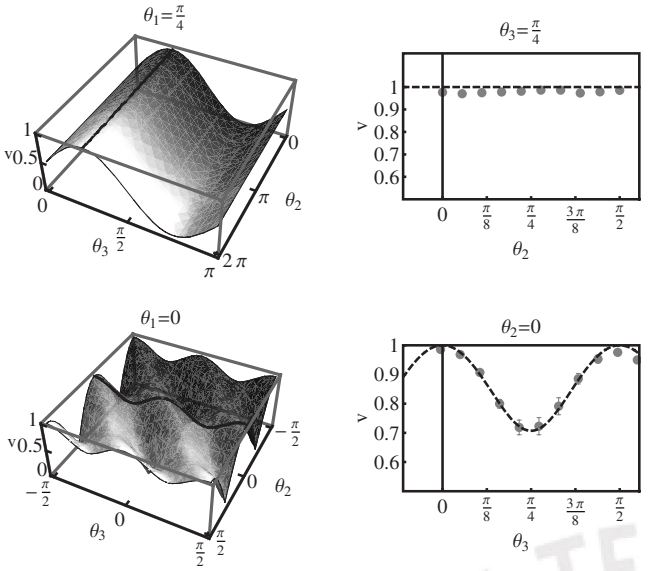

FIG. 6. Interferometric measurement of the visibility $v(\theta_1,\theta_2,\theta_3)$. The left panels show the surfaces obtained by fixing one of the three angles, θ_1, as indicated. The right panels show the experimental results that correspond to the curves highlighted on the surfaces. The upper curve is obtained by fixing θ_3 besides θ_1, while the lower curve is obtained by fixing θ_2 and θ_1. In the upper curve all experimental values fall below the predicted (maximal) visibility of 1. This is because $I_{\min}$ is never zero, as required to obtain $v=1$. By subtracting the nonzero average of $I_{\min}$ the experimental points would fall above and below the theoretical curve, as it occurs for the lower curve, which corresponds to $v<1$.

$\approx \mathrm{Im}\{\ln[i_{up}(k_0)]\}-\mathrm{Im}\{\ln[i_{low}(k_0)]\}$, up to a constant phase offset that is the same for all the interferograms pertaining to a given $U(\xi,\eta,\zeta)$. The above expression for Δ_r comes from observing that both $i_{up}(k_0)$ and $i_{low}(k_0)$ have the structure $i(k_0)=a(k_0)+b(0)\exp(i\Delta)+b^*(2k_0)\exp(-i\Delta)$, so that $i(k_0)\approx b(0)\exp(i\Delta)$ whenever $|b(0)|\gg|b^*(2k_0)|,|a(k_0)|$. Thus, the accuracy of the approximation for Δ_r depends on how well one can separate the Fourier components of $i(k_0)$. In the present case we applied this procedure only for the sake of checking our results. An attempt to systematize this method would be worth only if one's goals require an automated phase-retrieval method. In our case, as we were interested in giving a proof of principle only, the method of choice was not a fully automated one, but a partially manual method which was envisioned to demonstrate the feasibility of our approach.

Another series of tests was devoted to measuring the visibility v as given in Eq. (11). The quantity $v(\theta_1,\theta_2,\theta_3)$ was submitted to test by fixing two of its three arguments. Our results are shown in Fig. 6. The left panels correspond to $v(\theta_1,\theta_2,\theta_3)$ as a function of θ_2 and θ_3, that is, the surface obtained by fixing θ_1 as indicated. In the right panels we compare the theoretical predictions against our measurements of $v(\theta_1,\theta_2,\theta_3)$, whereby two of the three arguments have been held fixed. The interferograms were evaluated following a procedure similar to the one already explained. However, in this case it was not the full cross section of the beam that was submitted to evaluation, but a manually chosen region of the images corresponding to a part of the input beam having almost uniform intensity. This had to be so, because Eq. (11) presupposes a uniform profile of the input beam. In order to test the visibility of the whole cross section of the beam, Eq. (11) should be modulated with a Gaussian envelope. Such a refinement was however unnecessary for our scopes. In any case, the experimental value of the visibility, viz., $(I_{\max}-I_{\min})/(I_{\max}+I_{\min})$, was obtained by choosing in each interferogram several maxima and minima, so as to assess the accuracy of our measurements. Thus, the error bars in the figures take proper account of the tiny variations in the chosen region of the input-beam profile. As can be seen, the experimental values closely fit the theoretical predictions.

IV. CONCLUSIONS

We have carried out theoretical calculations and the corresponding measurements of Pancharatnam's phase by applying the polarimetric and the interferometric methods. Our interferometric array is robust against thermal and mechanical disturbances. It can be implemented with a Michelson, a Sagnac, or a Mach-Zehnder interferometer. We have compared our measurements with those obtained in a polarimetric array, finding similar results in both cases. Our polarimetric array consisted of five wave plates and two polarizers. Five plates are necessary to realize an arbitrary SU(2) transformation with the polarimetric array. As well known, three plates are instead required for realizing an arbitrary SU(2) transformation with an interferometric array. The whole Poincaré sphere of polarization states could be explored with both our polarimetric and interferometric arrays. Thus, any two given polarization states could be connected by the appropriate SU(2) transformation. The associated relative Pancharatnam's phase would thereby be realized. This phase can be decomposed as a sum of dynamical and geometrical phases. By appropriately choosing the path connecting two given states on the Poincaré sphere, one can study different aspects of both the dynamical and the geometrical phases.

We have also tested theoretical predictions concerning fringe visibility when applying the interferometric method. Our experimental findings were in very good agreement with theoretical predictions. This is interesting not only on its own, but also in view of extracting Pancharatnam's phase from visibility measurements in the case of mixed states. Indeed, it has been proved [18] that, for mixed states, fringe visibility is a simple function of Pancharatnam's phase.

ACKNOWLEDGMENTS

We wish to thank E. J. Galvez for his technical advice and for kindly lending us some optical equipments. This work was partially supported by DAI-PUCP (Contract No. DAI-2009-0010). R.W. acknowledges financial support from the Deutsche Forschungsgemeinschaft (Contracts No. WI 393/20-1 and No. WI 393/21-1).

[1] S. Pancharatnam, Proc. Indian Acad. Sci., A **44**, 247 (1956).
[2] M. V. Berry, J. Mod. Opt. **34**, 1401 (1987).
[3] A. Tomita and R. Y. Chiao, Phys. Rev. Lett. **57**, 937 (1986).
[4] R. Bhandari and J. Samuel, Phys. Rev. Lett. **60**, 1211 (1988).
[5] T. H. Chyba, L. J. Wang, L. Mandel, and R. Simon, Opt. Lett. **13**, 562 (1988).
[6] A. G. Wagh, V. C. Rakhecha, J. Summhammer, G. Badurek, H. Weinfurter, B. E. Allman, H. Kaiser, K. Hamacher, D. L. Jacobson, and S. A. Werner, Phys. Rev. Lett. **78**, 755 (1997).
[7] A. G. Wagh, G. Badurek, V. C. Rakhecha, R. J. Buchelt, and A. Schricker, Phys. Lett. A **268**, 209 (2000).
[8] A. G. Wagh and V. C. Rakhecha, Pramana **63**, 51 (2004).
[9] A. G. Wagh and V. C. Rakhecha, Phys. Lett. A **197**, 112 (1995).
[10] A. G. Wagh and V. C. Rakhecha, Phys. Lett. A **197**, 107 (1995).
[11] V. C. Rakhecha and V. G. Wagh,Pramana, J. Phys. **56**, 287 (2001).
[12] M. Ericsson, D. Achilles, J. T. Barreiro, D. Branning, N. A. Peters, and P. G. Kwiat, Phys. Rev. Lett. **94**, 050401 (2005).
[13] R. Simon and N. Mukunda, Phys. Lett. A **143**, 165 (1990).
[14] B.-G. Englert, C. Kurtsiefer, and H. Weinfurter, Phys. Rev. A **63**, 032303 (2001).
[15] W. P. Schleich, *Quantum Optics in Phase Space* (Wiley-VCH, Berlin, 2001).
[16] R. Simon and N. Mukunda, Phys. Lett. A **138**, 474 (1989).
[17] K. A. Goldberg and J. Bokor, Appl. Opt. **40**, 2886 (2001).
[18] E. Sjöqvist, A. K. Pati, A. Ekert, J. S. Anandan, M. Ericsson, D. K. L. Oi, and V. Vedral, Phys. Rev. Lett. **85**, 2845 (2000).

Pancharatnam and Geometric Phases

Omar Ortiz

PUCP

2016

Pancharatnam's phase

Pancharatnam prescribed how to determine when two polarizations states were in phase

$$\textit{phase difference between } |A\rangle \textit{ and } |B\rangle = \textit{ phase of } \langle A|B\rangle$$

$$\langle A|B\rangle = |\langle A|B\rangle| \exp(i\phi)$$

$$\phi = \textit{Pancharatnam's phase} = \phi_P$$

Pancharatnam's phase: Interferometry

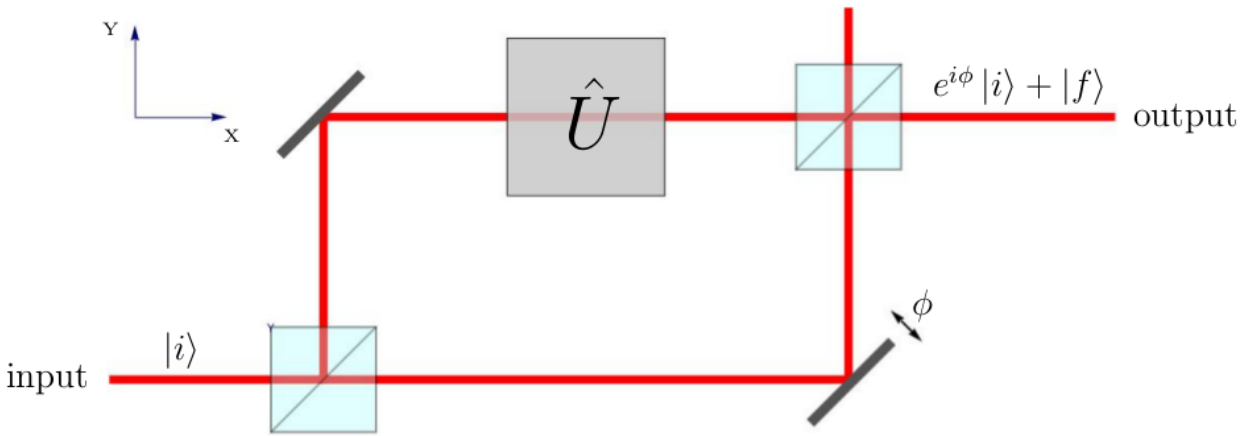

Intensity at the output can be written as

$$\begin{aligned} I &\propto 1 + v\cos(\phi - \Phi_P) \\ \textit{visibility} &: v = |\langle i|f\rangle| \\ \textit{Pancharatnam's phase} &: \Phi_P = \arg\langle i|f\rangle \end{aligned}$$

where

$$|f\rangle = U|i\rangle$$

Pancharatnam's phase: Interferometry

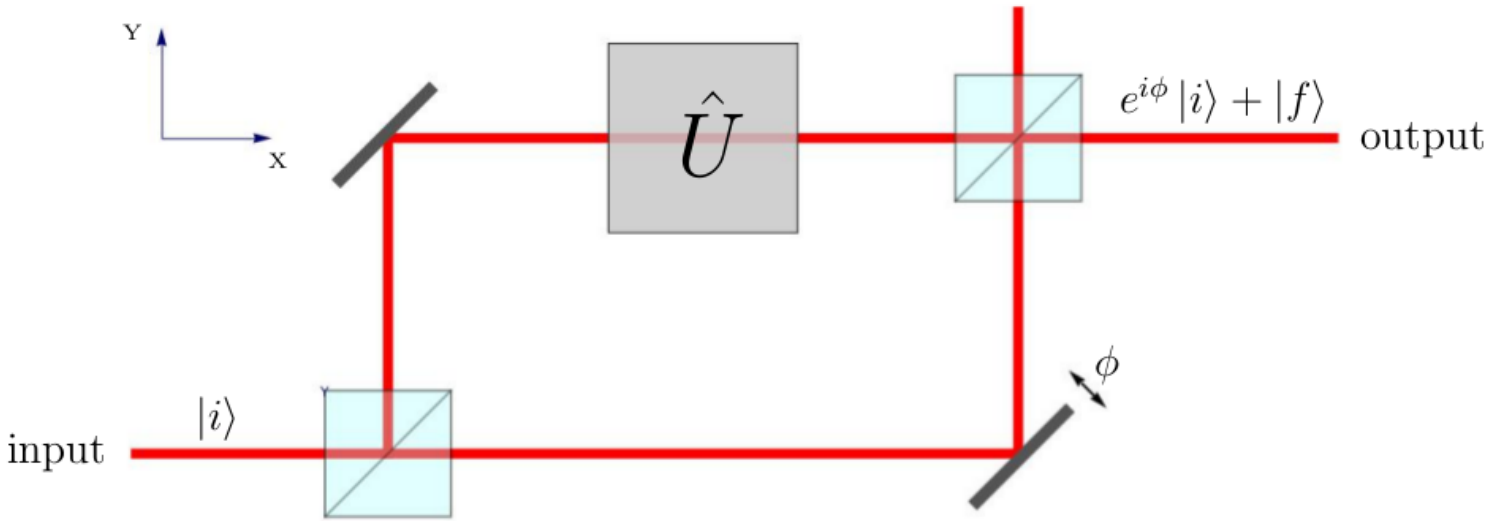

Instabilities in the interferometer overshadow Pancharatnam's phase. We explore solutions using Sagnac interferometry and close-loop phase-locked interferometer.

Pancharatnam's phase: Interferometry

Final version of our setup

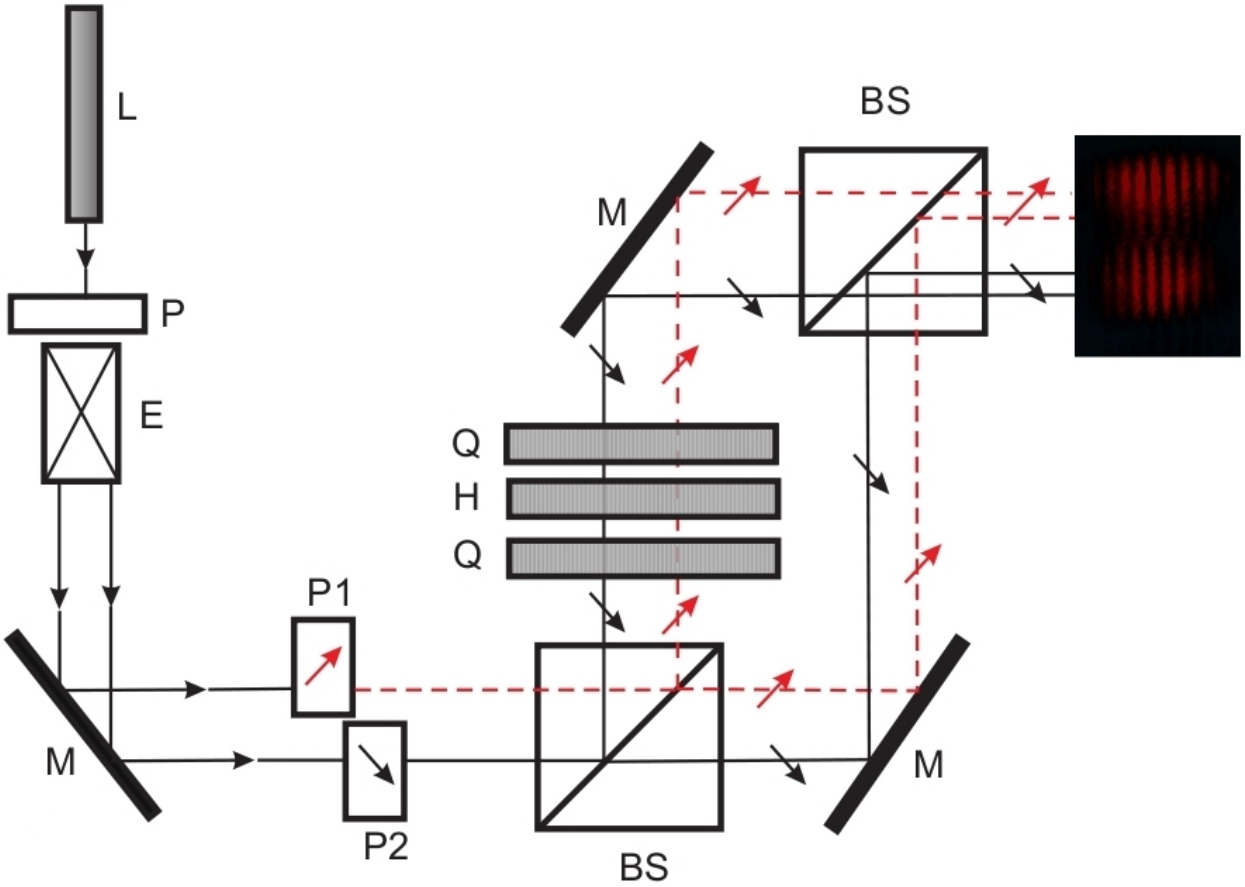

Pancharatnam's phase: Interferometry

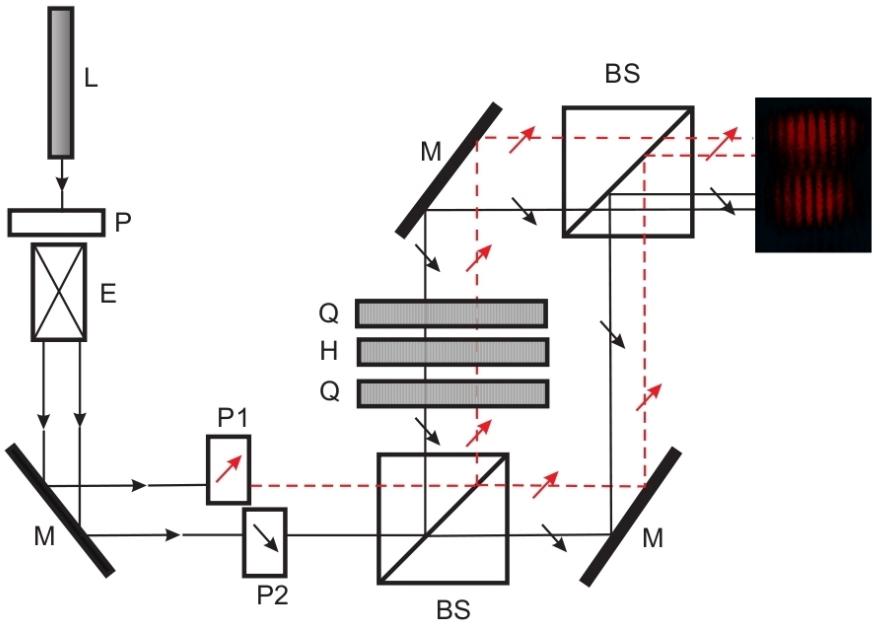

Vertical and horizontal polarized beams produce interferograms associated with the following expressions for intensity

$$I_V = \frac{1}{2}[1 - \cos(\beta)\cos(\phi - \delta)]$$

$$I_H = \frac{1}{2}[1 - \cos(\beta)\cos(\phi + \delta)]$$

Pancharatnam's phase: Interferometry

Considering the final state $|f\rangle = \hat{U}_{zyz}\,|i\rangle$ for $i = H, V$ resulting from applying a SU(2) transformation parametrized as

$$\hat{U}_{zyz}(\beta,\gamma,\delta) = \exp(i\frac{\delta+\gamma}{2}\hat{\sigma}_z)\exp(i\beta\hat{\sigma}_y)\exp(i\frac{\delta-\gamma}{2}\hat{\sigma}_z)$$

it can be proved that for $i = H$

$$\phi_P = \delta$$

Pancharatnam's phase: Interferometry

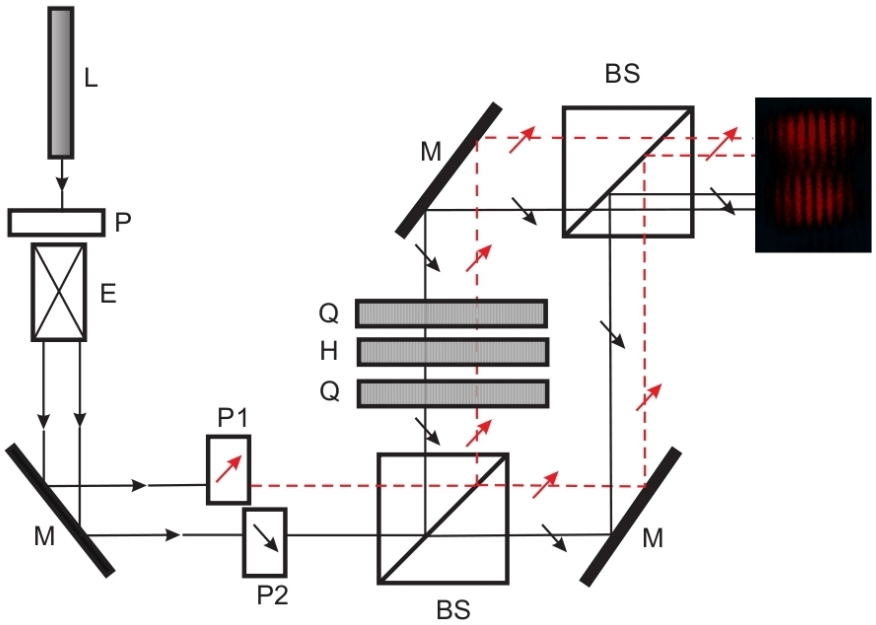

Vertical and horizontal polarized beams produce interferograms associated with the following expressions for intensity

$$I_V = \frac{1}{2}[1 - \cos(\beta)\cos(\phi - \delta)]$$

$$I_H = \frac{1}{2}[1 - \cos(\beta)\cos(\phi + \delta)]$$

Pancharatnam's phase: Interferometry

Pancharatnam's phase can be measured by comparison of the two interferograms

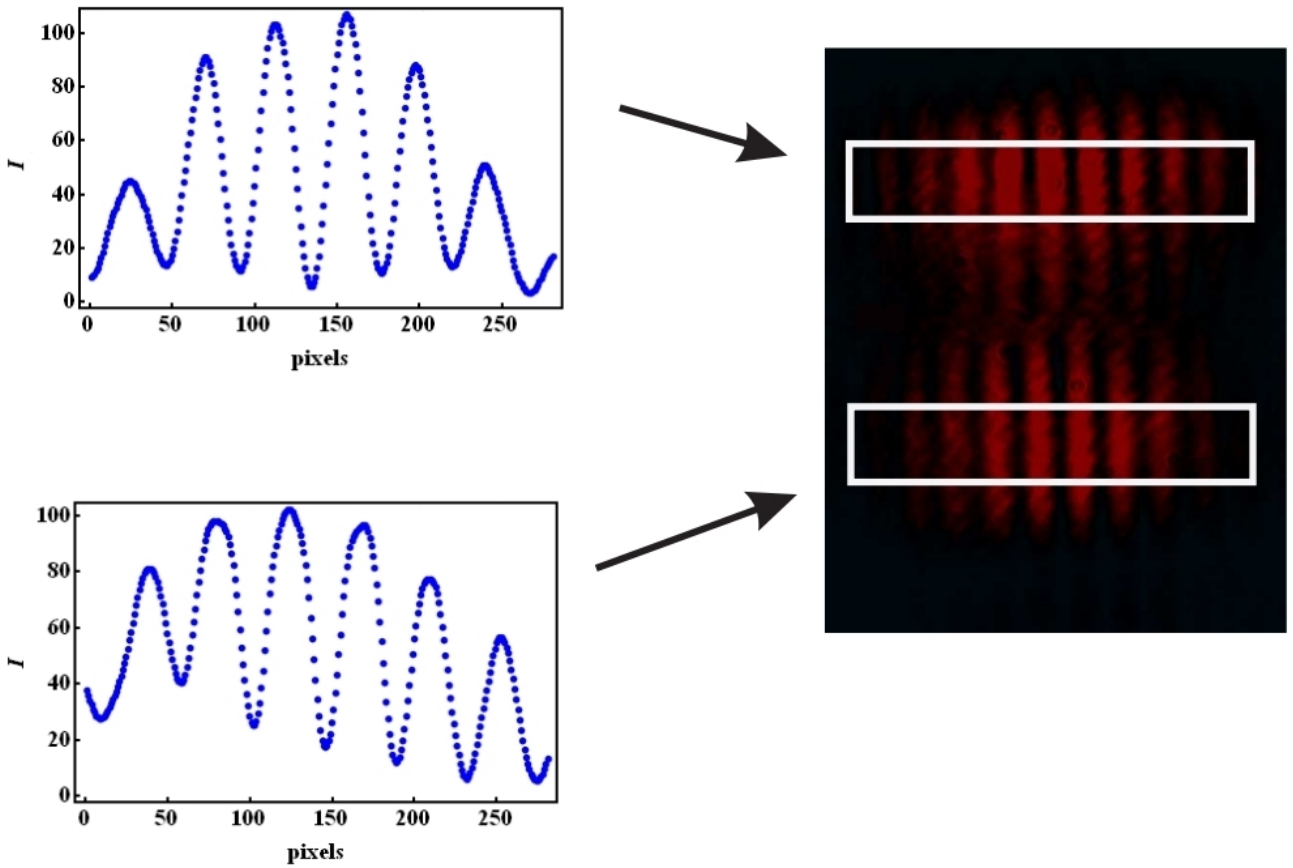

Pancharatnam's phase: Interferometry

Final state $|f\rangle = \hat{U}_{yzy}\,|i\rangle$ for $i = H, V$ results from applying SU(2) transformation:

$$\hat{U}_{yzy}(\xi,\eta,\zeta) = \exp(-i\frac{\xi}{2}\hat{\sigma}_y)\exp(i\frac{\eta}{2}\hat{\sigma}_z)\exp(-i\frac{\zeta}{2}\hat{\sigma}_y)$$

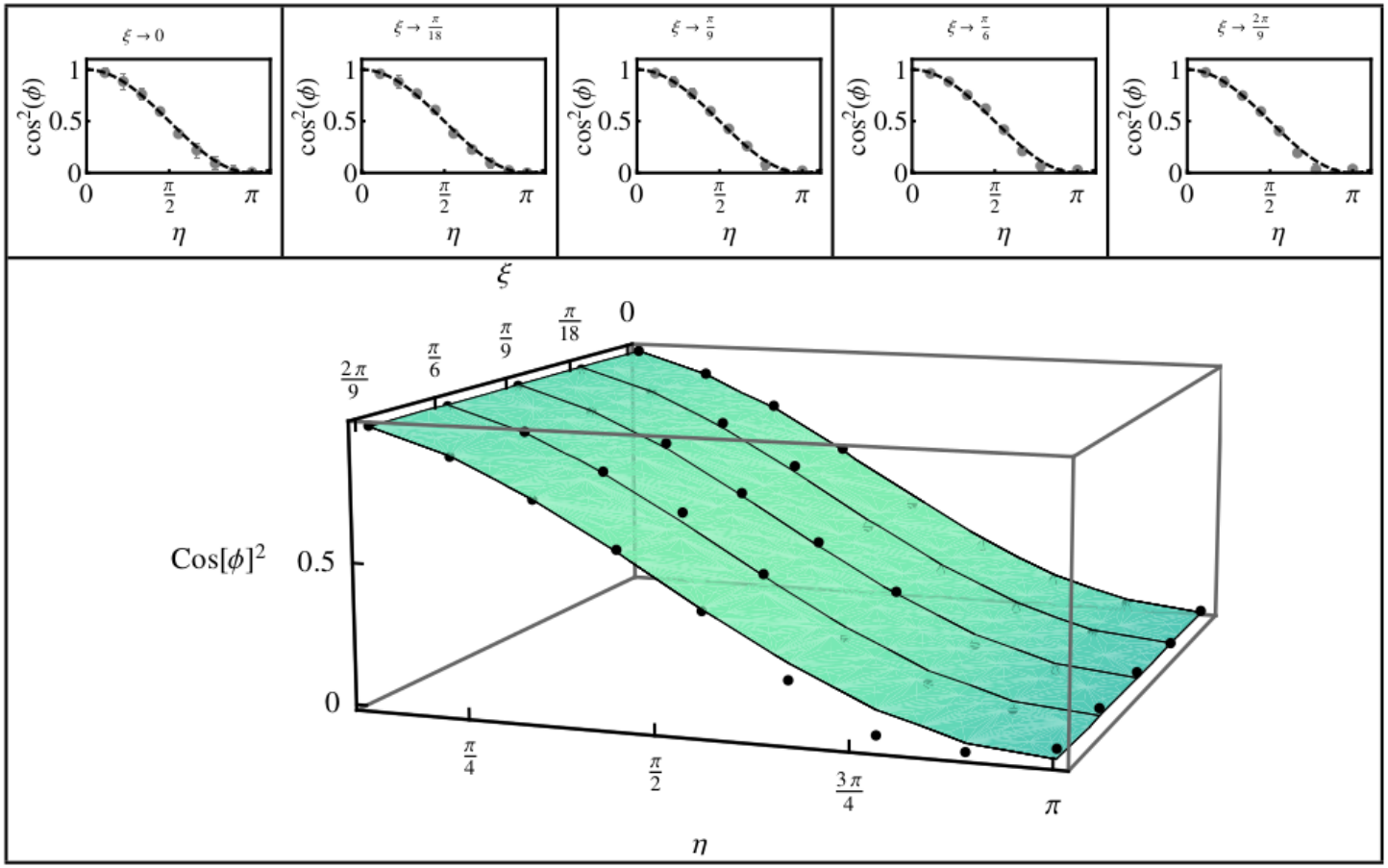

Pancharatnam's phase: Interferometry

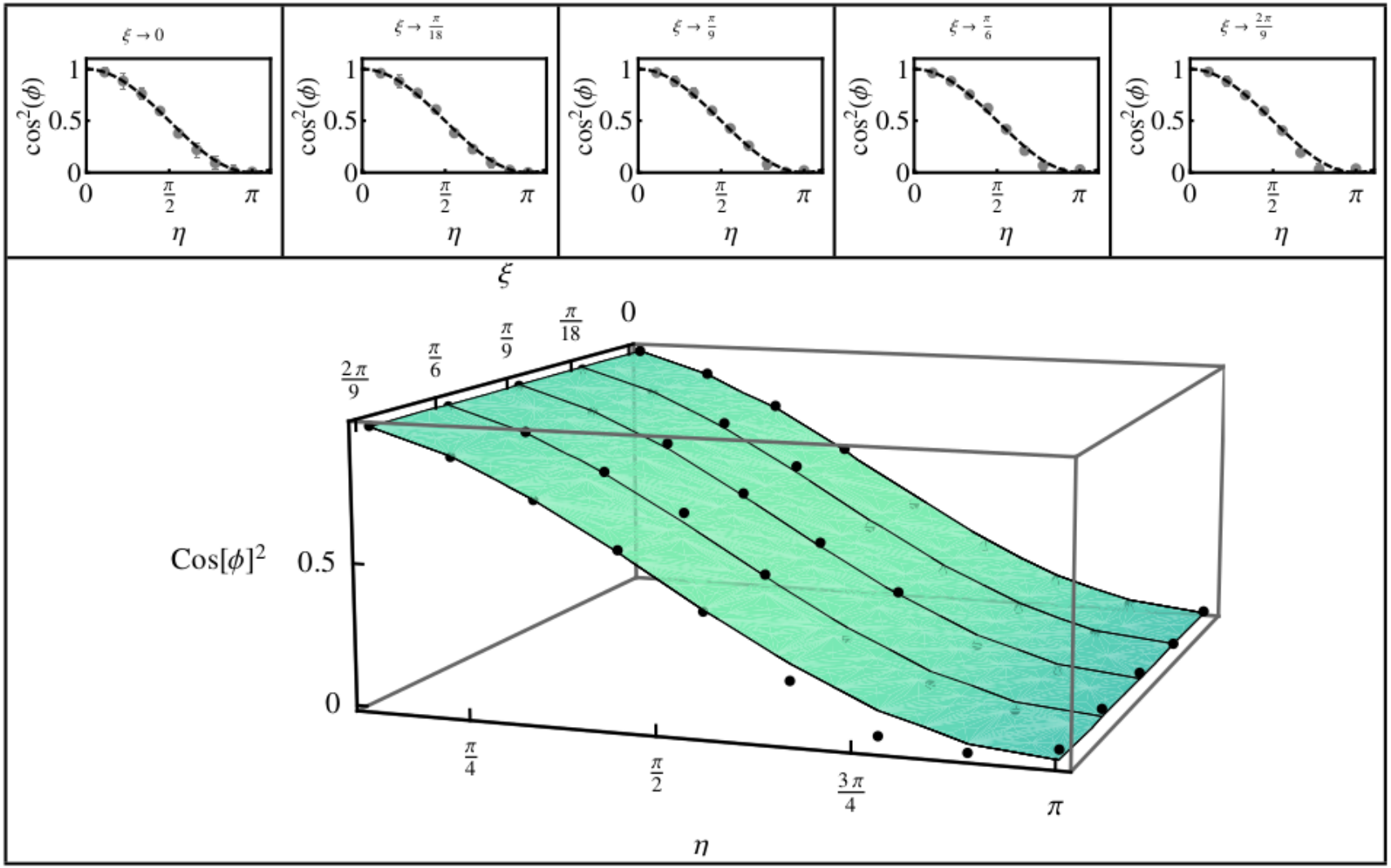

Pancharatnam's phase: Polarimetry (virtual interferometry)

An analogy is possible between operators acting on momentum dof and polarization dof

$$\hat{U}_{BS}^{pol} = H(\pi/8) = -\frac{i}{\sqrt{2}}\begin{pmatrix} 1 & 1 \\ 1 & -1 \end{pmatrix}$$

$$\hat{U}_{\phi}^{pol} = Q(\pi/4)H(-\frac{\phi+\frac{\pi}{2}}{2})Q(\pi/4) = \begin{pmatrix} e^{i\phi} & 0 \\ 0 & e^{-i\phi} \end{pmatrix}$$

Pancharatnam's phase: Polarimetry (virtual interferometry)

With this result we can build our virtual interferometer as

$$\hat{U}_{int} = \hat{U}_{BS}^{pol}\ \hat{U}_{zyz}\ \hat{U}_{\phi}^{pol}\ \hat{U}_{BS}^{pol}$$

then

$$I = |\langle H|\,\hat{U}_{int}\,|H\rangle| = \cos^2(\beta)\cos^2(\delta) + \sin^2(\beta)\cos^2(\gamma+\phi)$$

which allows us to measure Pancharatnam phase using only the maximun and minimun values of intensity

$$\cos^2(\Phi_P) = \cos^2(\delta) = \frac{I_{min}}{1 - I_{max} - I_{min}}$$

Pancharatnam's phase: Polarimetry, virtual interferometry

Our final setup looks as follows

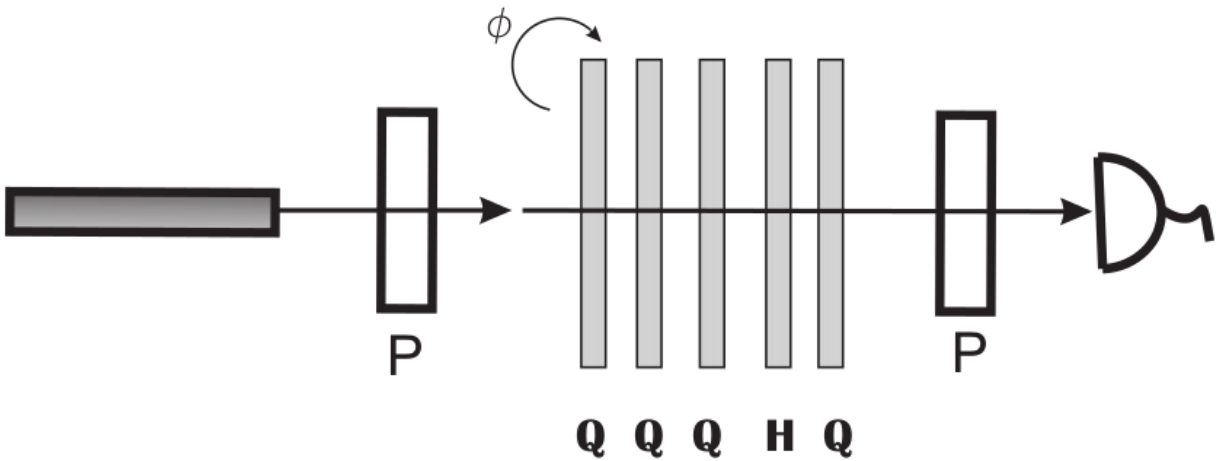

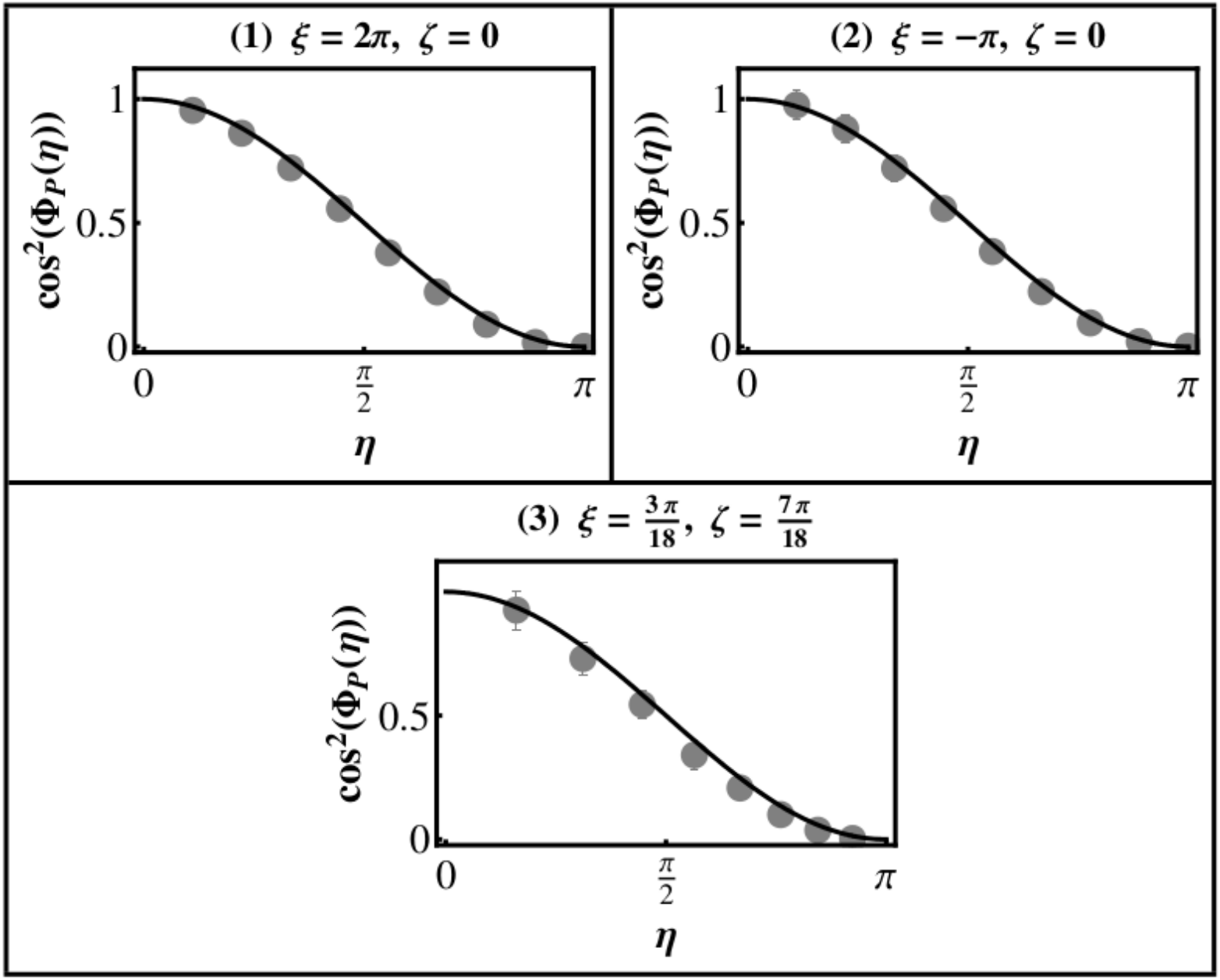
(1) $\xi = 2\pi,\ \zeta = 0$
$\cos^2(\Phi_P(\eta))$
1
0.5
0
0
$\frac{\pi}{2}$
π
η
(2) $\xi = -\pi,\ \zeta = 0$
$\cos^2(\Phi_P(\eta))$
1
0.5
0
0
$\frac{\pi}{2}$
π
η
(3) $\xi = \frac{3\pi}{18},\ \zeta = \frac{7\pi}{18}$
$\cos^2(\Phi_P(\eta))$
0.5
0
0
$\frac{\pi}{2}$
π
η

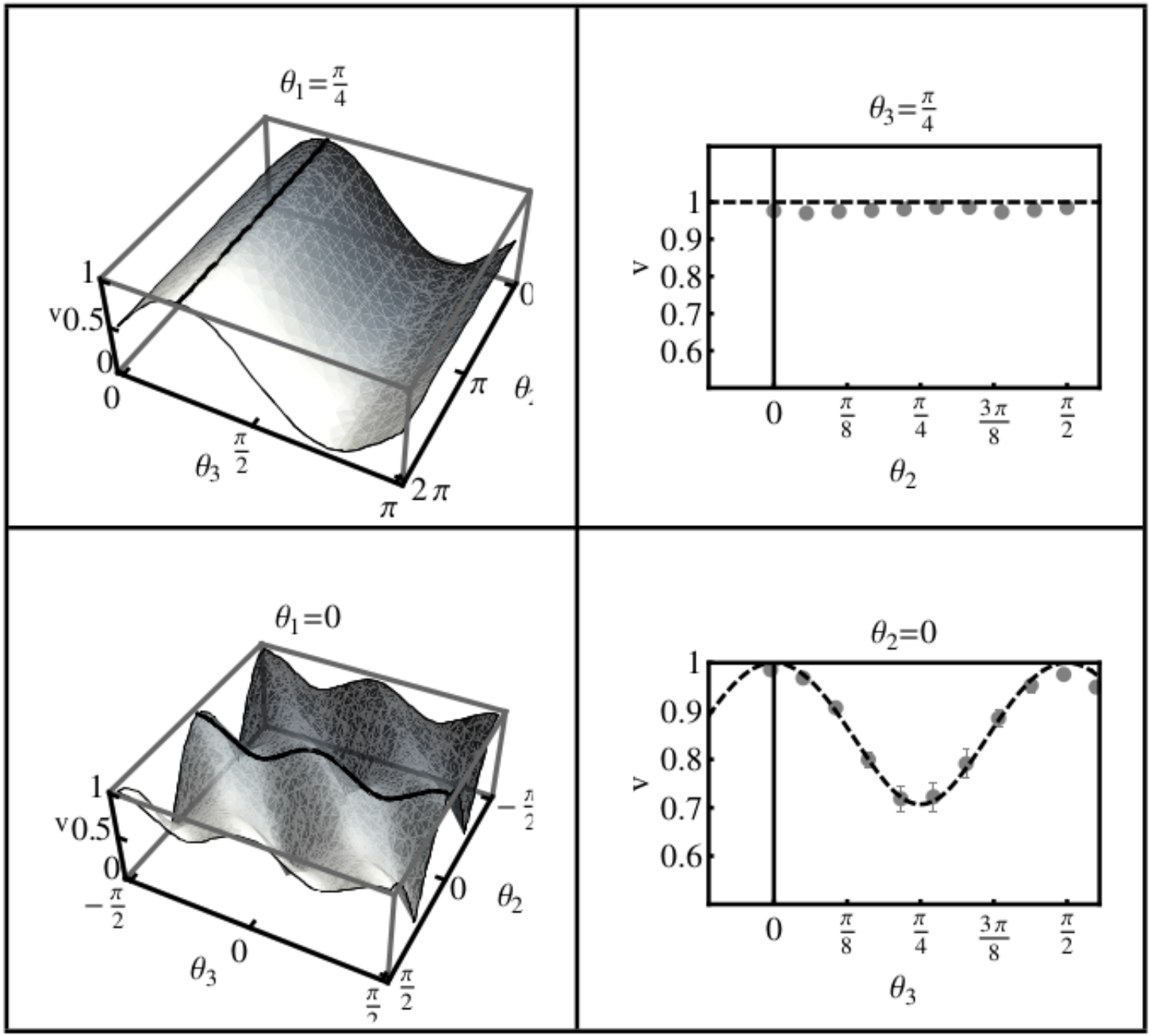
$\theta_1=\frac{\pi}{4}$
v
1
0.5
0
0
θ_3
$\frac{\pi}{2}$
π
2π
π
θ_2
$\theta_3=\frac{\pi}{4}$
v
1
0.9
0.8
0.7
0.6
0
$\frac{\pi}{8}$
$\frac{\pi}{4}$
$\frac{3\pi}{8}$
$\frac{\pi}{2}$
θ_2
$\theta_1=0$
v
1
0.5
0
$-\frac{\pi}{2}$
θ_3
0
$\frac{\pi}{2}$
$\frac{\pi}{2}$
0
θ_2
$\theta_2=0$
v
1
0.9
0.8
0.7
0.6
0
$\frac{\pi}{8}$
$\frac{\pi}{4}$
$\frac{3\pi}{8}$
$\frac{\pi}{2}$
θ_3

Geometric phase

Kinematic definition of geometric phase (Mukunda and Simon)

$$\phi_g = \underbrace{\arg \langle \Psi_{(s_i)} | \Psi_{(s)} \rangle}_{\phi_P} - \underbrace{\int_{s_i}^{s} Im \langle \Psi_{(s)} | \dot{\Psi}_{(s)} \rangle \, ds}_{\phi_{dyn}}$$

ϕ_g is invariant under local phase changes

$$|\Psi'(s)\rangle = e^{i\alpha(s)} |\Psi(s)\rangle$$

$$\phi'_g = \phi_g$$

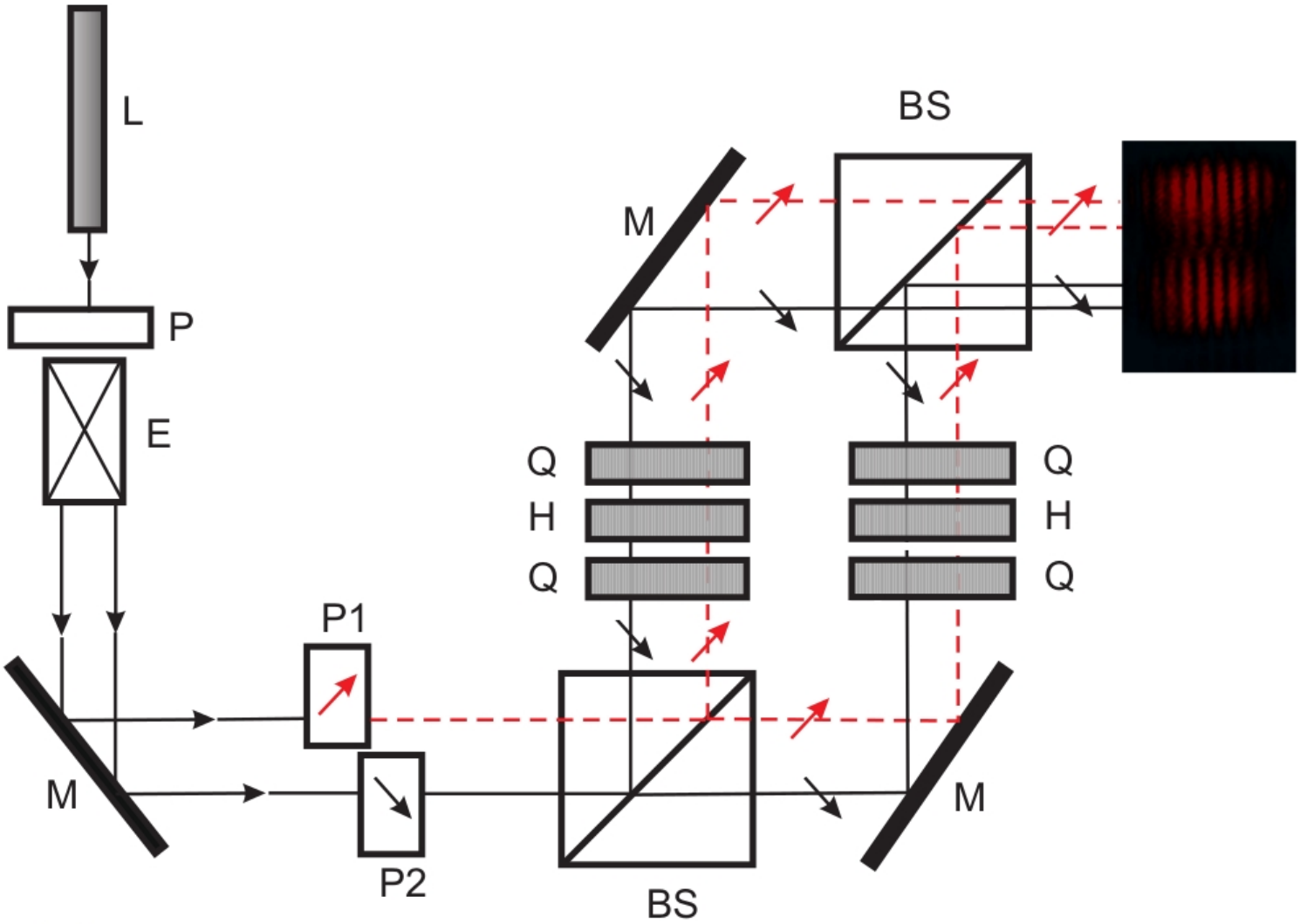
L
P
E
M
P1
P2
BS
Q
H
Q
BS
M
Q
H
Q
M

$\mathrm{n} = (\frac{3}{5}, \frac{4}{5}, 0) \qquad \beta = 53^o$

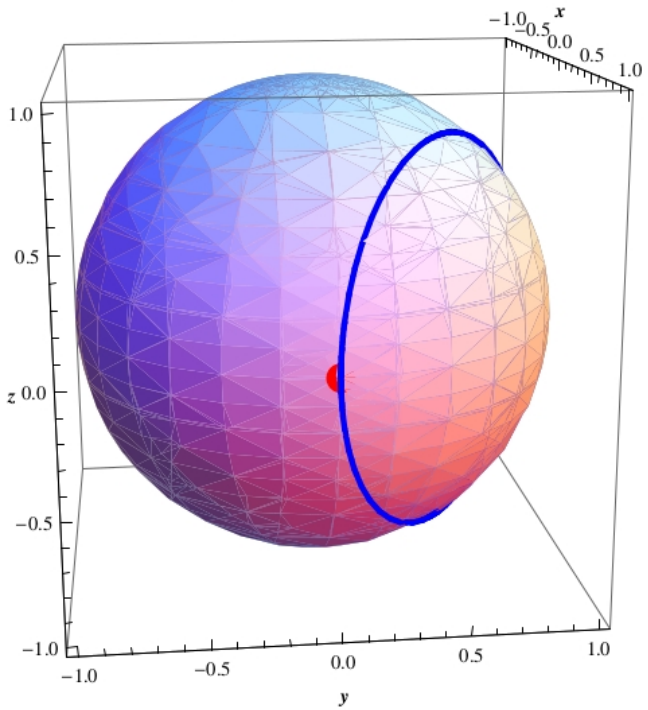

$\mathrm{n} = (\frac{3}{5}, \frac{4}{5}, 0) \qquad \beta = 53^o$

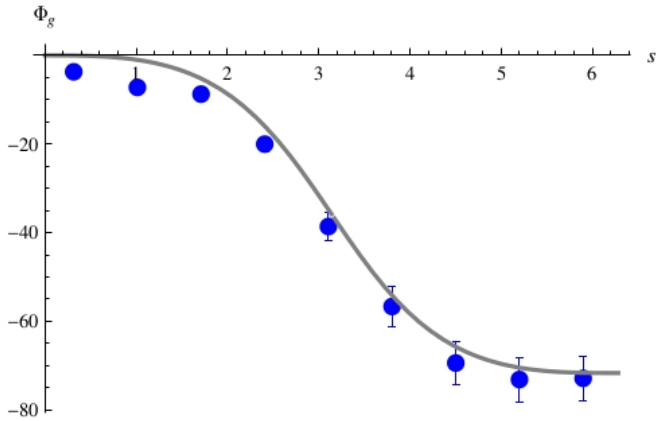

$\mathrm{n} = (-\frac{1}{2}, \frac{\sqrt{3}}{2}, 0) \qquad \beta = 120^o$

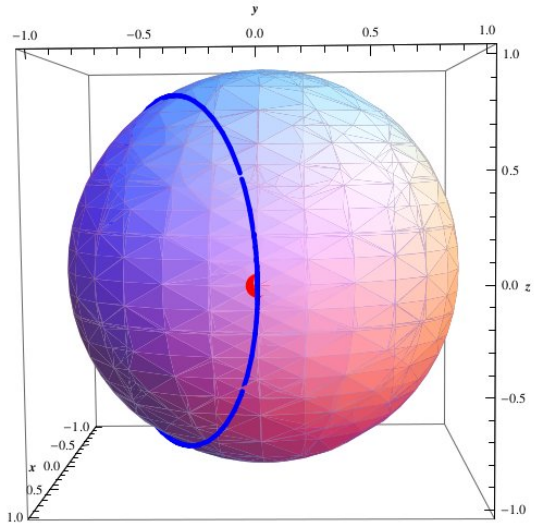

$\mathrm{n} = (-\frac{1}{2}, \frac{\sqrt{3}}{2}, 0) \qquad \beta = 120^o$

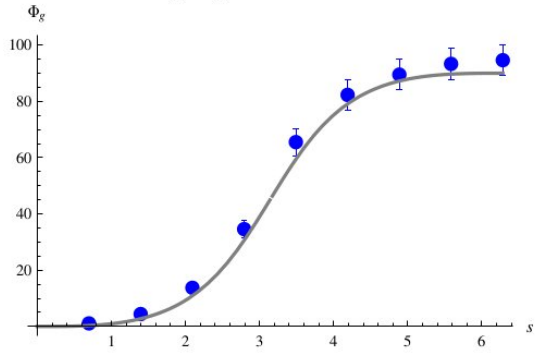

$\mathrm{n} = (\frac{1}{2}, \frac{\sqrt{3}}{2}, 0) \qquad \beta = 60^o$

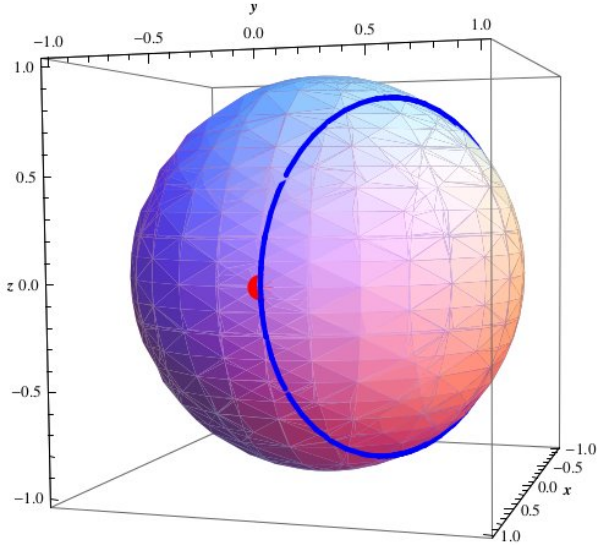

$\mathrm{n} = (\frac{1}{2}, \frac{\sqrt{3}}{2}, 0) \qquad \beta = 60^o$

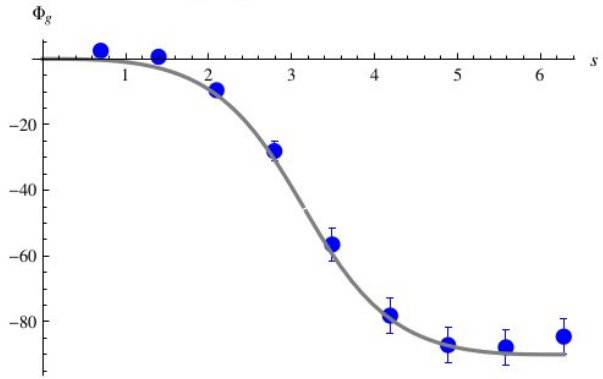

Polarimetric measurements of single-photon geometric phases

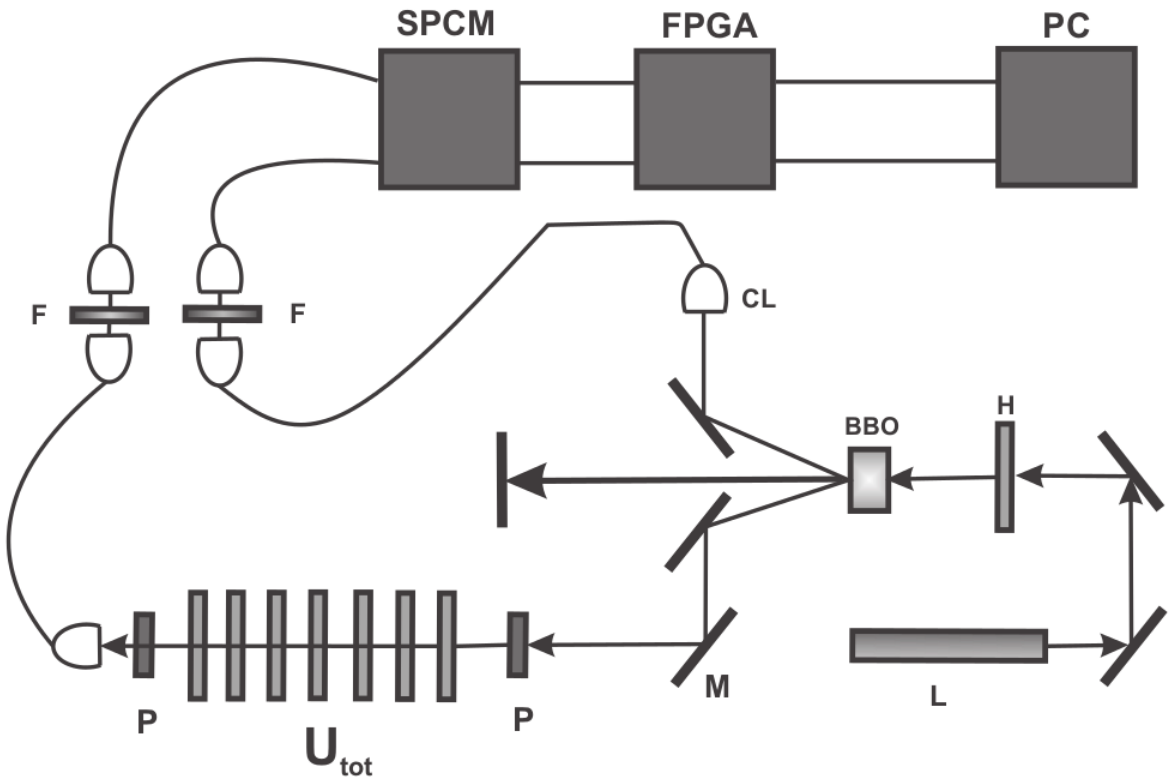

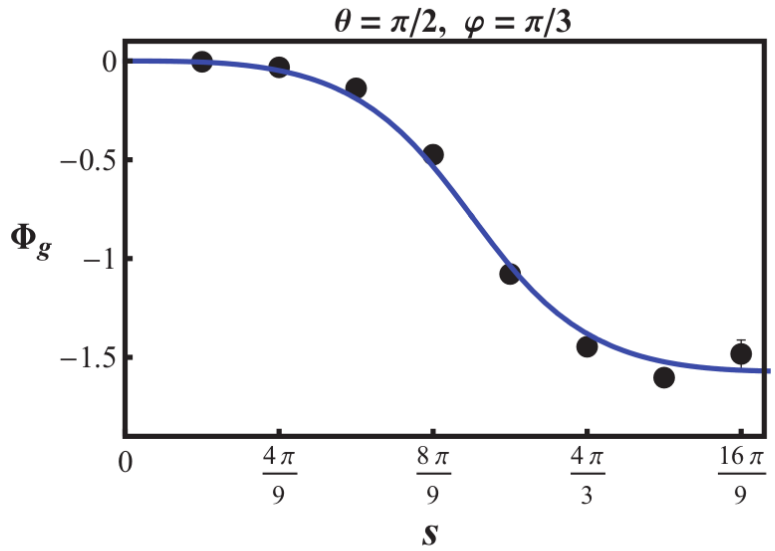
$\theta = \pi/2,\ \varphi = \pi/3$
0
−0.5
−1
−1.5
Φ_g
0
$\frac{4\pi}{9}$
$\frac{8\pi}{9}$
$\frac{4\pi}{3}$
$\frac{16\pi}{9}$
s

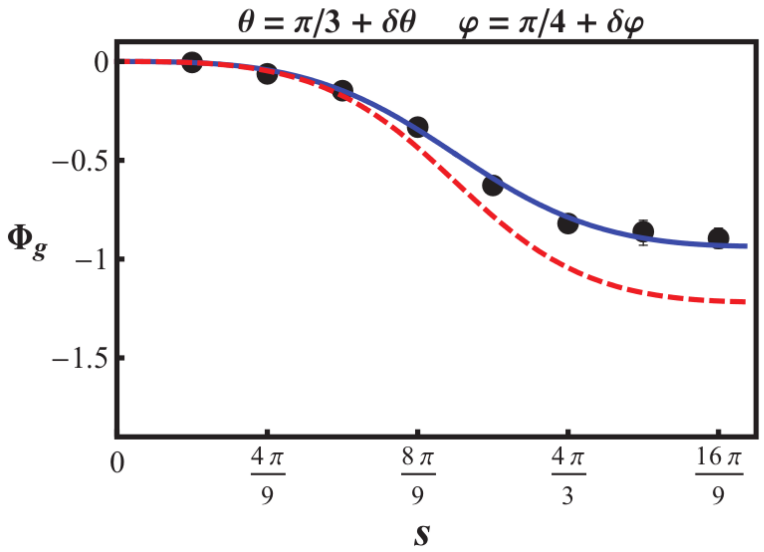
$\theta = \pi/3 + \delta\theta \quad \varphi = \pi/4 + \delta\varphi$
0
−0.5
−1
−1.5
Φ_g
0
$\frac{4\pi}{9}$
$\frac{8\pi}{9}$
$\frac{4\pi}{3}$
$\frac{16\pi}{9}$
s

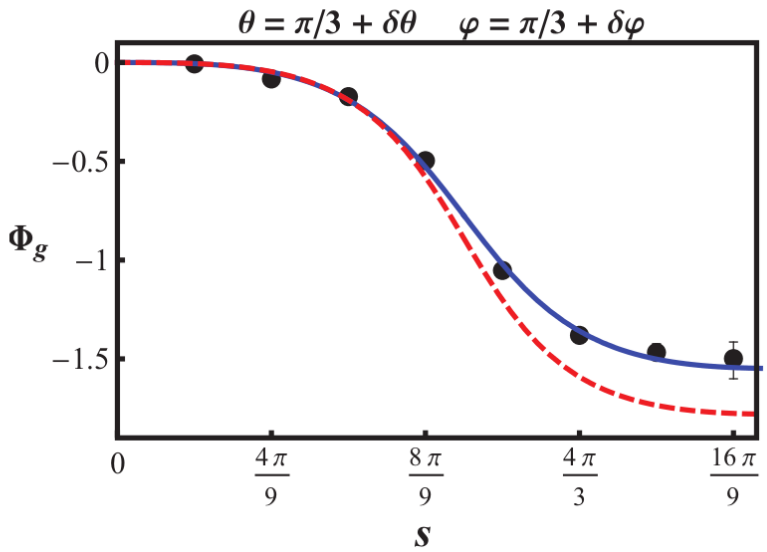
$\theta = \pi/3 + \delta\theta \quad \varphi = \pi/3 + \delta\varphi$
0
−0.5
−1
−1.5
Φ_g
0
$\frac{4\pi}{9}$
$\frac{8\pi}{9}$
$\frac{4\pi}{3}$
$\frac{16\pi}{9}$
s

Conclusions

- We have implemented robust interferometric arrays for measuring Pancharatnam and geometric phases.
- We have exhibited inherently robust and very versatile polarimetric arrays for generating Pancharatnam and geometric phases.
- Our setups work with both classical light (laser) and quantum light (single photons)